Cerebral Cortex September 2006;16:1289–1295
doi:10.1093/cercor/bhj071
Advance Access publication November 9, 2005

Brain Processing of the Signals Ascending Through Unmyelinated C Fibers in Humans: An Event-Related Functional Magnetic Resonance Imaging Study

Yunhai Qiu[1,3], Yasuki Noguchi[1,3], Manabu Honda[2,3,4], Hiroki Nakata[1,3], Yohei Tamura[1], Satoshi Tanaka[2,3], Norihiro Sadato[2,3,4], Xiaohong Wang[1], Koji Inui[1,3] and Ryusuke Kakigi[1,3,5]

[1]Department of Integrative Physiology and [2]Division of Cerebral Integration, National Institute for Physiological Sciences, Myodaiji, Okazaki 444-8585, Japan, [3]Department of Physiological Sciences, School of Life Sciences, The Graduate University for Advanced Studies, Hayama, Kanagawa 240-0193, Japan and [4]SORST and [5]RISTEX, Japan Science and Technology Corp Agency (JST), Kawaguchi 332-0012, Japan

Event-related functional magnetic resonance imaging was used to investigate brain processing of the signals ascending from peripheral C and Aδ fibers evoked by phasic laser stimuli on the right hand in humans. The stimulation of both C and Aδ nociceptors activated the bilateral thalamus, bilateral secondary somatosensory cortex, right (ipsilateral) middle insula, and bilateral Brodmann's area (BA) 24/32, with the majority of activity found in the posterior portion of the anterior cingulate cortex (ACC). However, magnitude of activity in the right (ipsilateral) BA32/8/6, including dorsal parts in the anterior portion of the ACC (aACC) and pre-supplementary motor area (pre-SMA), and the bilateral anterior insula was significantly stronger following the stimulation of C nociceptors than Aδ nociceptors. It was concluded that the activation of C nociceptors, related to second pain, evokes different brain processing from that of Aδ nociceptors, related to first pain, probably due to the differences in the emotional and motivational aspects of either pain, which are mainly related to the aACC, pre-SMA, and anterior insula.

Keywords: ACC (anterior cingulate cortex), Aδ fiber, C fiber, fMRI, pain

Introduction

Generally, acute pain is classified as first and second pain associated with rapidly conducting Aδ fibers and slowly conducting unmyelinated C fibers, respectively. First pain aims at achieving relative safety from the source of injury, whereas second pain, with its strong affective component, attracts longer lasting attention and initiates behavioral responses in order to limit further injury and optimize recovery (Wall 1979; Ploner and others 2002). Accordingly, the distinct brain representations for first and second pain should reflect distinct biological functions of both sensations.

Because a phasic painful laser pulse can produce brain responses related to first pain (Mor and Carmon 1975), pain perception in humans has been intensively investigated in neuroimaging studies using positron emission tomography (PET) and functional magnetic resonance imaging (fMRI). Using conventional laser stimuli, these studies showed activations in multiple regions such as the primary somatosensory cortex (SI), secondary somatosensory cortex (SII), insula cortex, and cingulate cortex (Svensson and others 1997; Xu and others 1997; Mauguiere and others 1999; Sawamoto and others 2000; Bingel and others 2002; Bornhovd and others 2002; Buchel and others 2002; Bingel, Glascher, and others 2004; Bingel, Lorenz, and others 2004). However, the differential brain responses to signals ascending from peripheral Aδ and C fibers are unclear and remain to be investigated because these neuroimaging studies only investigated brain processing on the activation of Aδ nociceptors. Although painful laser pulses activate concomitantly Aδ and C nociceptors, it was very difficult or impossible to activate C nociceptors independently using laser stimulation (Bromm and Treede 1984).

To examine brain processing related to the activation of C nociceptors, capsaicin injection has been employed in a few neuroimaging studies using PET and fMRI. However, capsaicin is associated with the stimulation of not only C nociceptors but also Aδ nociceptors (Holzer 1991; Szallasi 1994), and the responses it evokes reflect a mixture of bottom-up and top-down processes and complex pain-coping strategies, as well as perceptual and physiological phenomena like temporal summation (Price and others 1977) and wind up (Mendell and Wall 1965) because capsaicin induces long-lasting tonic pain. Therefore, using phasic (short lasting) stimulation to selectively activate C nociceptors is more suitable to the study of brain processing based on identification of the onset period for laser stimuli and fMRI scans than tonic capsaicin-induced stimulation.

Recently, a Belgian group (Bragard and others 1996; Opsommer and others 1999) developed a new method for selectively stimulating C nociceptors using a laser pulse applied to a tiny area of skin and succeeded in recording laser-evoked potentials (LEPs) related to the activation of C nociceptors (Plaghki and Mouraux 2003). The physiological background of this method is that the C nociceptors in the skin have a higher density than the Aδ nociceptors (Ochoa and Torebjork 1989; Schmidt and others 1994; Treede and others 1994). We adopted this new approach by arranging the stimulus method. We used an aluminum plate with many holes whereas the Belgian group used a plate with 1 hole attached at the top of the laser stimulation probe. We concluded that this method selectively activates C nociceptors based on studies using microneurography (Qiu and others 2003), electroencephalography (EEG) (Qiu and others 2001, 2002; Tran and others 2001; Tran and others 2003), and magnetoencephalography (Tran and others 2002; Qiu and others 2004).

In this study, we used fMRI to identify brain activity evoked by the stimulation of C nociceptors using an aluminum plate with numerous holes in healthy human subjects. We also used fMRI following the activation of Aδ nociceptors with a conventional method (without using the aluminum spatial filter) to compare the results between the 2 methods. This procedure should demonstrate the distinct brain responses reflecting different biological functions of both first and second pain.

Methods

Subjects

Thirteen healthy male volunteers (1 left handed) participated in this study. They ranged in age from 25 to 39 (mean ± standard deviation: 30.9 ± 4.3). This study was approved by the Ethics Committee at our Institute, and all participants gave their informed consent. None of the

subjects suffered from diseases that might affect normal somatosensory and pain perception. During scanning, 1 investigator stayed with the subject in the scanner room and applied the laser stimuli to the dorsum of the right hand.

Stimulation of C and Aδ Nociceptors

A Tm:YAG laser stimulator (Carl Baasel Lasertech, Starnberg, Germany) was used to apply brief radiant pulses to the skin of the subjects with a wavelength of 1960 nm, a pulse duration of 1 ms, and a spot diameter of 3 mm. For stimulating C nociceptors, we used a thin aluminum plate attached to the top of the stimulus probe (distal end of laser optical fiber) as a spatial filter. This filter was 0.1 mm in depth, and in an area of 10×10 mm^2 on this plate, parallel lines were drawn every 1 mm, giving 11×11 intersections. A total of 121 (11×11) thin holes were drilled at these intersections, each with a diameter of 0.4 mm, corresponding to an area of 0.125 mm^2 for each hole. The laser pulse penetrated 7–11 holes on average. This aluminum spatial filter was placed as close as possible (less than 2 mm) above the skin to reduce the effect of diffraction. The principle of this method was based on that of previous studies (see Kakigi and others 2003; Plaghki and Mouraux 2003). For stimulating Aδ nociceptors, we used conventional laser stimuli without using the aluminum spatial filter. Because stimulus duration was very short, 1 ms, subjects felt a sharp (Aδ fibers stimulation) and burning or dull (C fibers stimulation) pain for a short period.

Before fMRI scanning, we determined the stimulus intensity for each subject by recording LEPs by averaging EEG. Bragard and others (1996) used 2 different laser strengths for activating C nociceptors, one weaker than and one the same as that for Aδ nociceptors, and recorded similar LEP findings between them. However, to minimize the effect of a difference of laser strength, we used the same laser strength for activating C and Aδ nociceptors, though the energy absorbed in the skin might not be exactly the same because of the spatial filter used for activating C nociceptors. The laser strength was determined as the weakest that could evoke clear LEPs following the stimulation of both C (using a thin aluminum plate) and Aδ (conventional method) nociceptors in each subject to minimize skin damage and discomfort (Qiu and others 2004). The mean intensity was 159.6 mJ, ranging from 145.0 to 180.0 mJ. The mean peak latency of the main positive component of LEPs following the stimulation of Aδ and C nociceptors was 351.1 and 932.2 ms, respectively. Using this procedure, we had confirmed that the present stimulus method was appropriate before recording fMRI.

Experimental Paradigm and Imaging Acquisition

The experiment was performed on 2 different days, with the second experiment performed 7 days after the first. In the first experiment, the 13 subjects were randomly separated into 2 groups, one assigned to the examination that stimulated C nociceptors, the other assigned to the examination that stimulated Aδ nociceptors. During the second experiment, these groups were switched. The event-related (single-event) design was used in this study. During the fMRI scans, the laser for either Aδ or C stimulation was applied to the right hand of subjects. The interstimulus interval between adjacent stimuli was either 14, 16, or 18 s, and these intervals were controlled with stimulus presentation software (Presentation 0.50, Neurobehavioral Systems, Albany, California). The fMRI scans were acquired using blood oxygenation level-dependent contrast T2*-weighted gradient echo. A total of 248 fMRI scans per session were acquired using echo-planar imaging sequences (time of repetition [TR], 2 s; echo time [TE], 30ms; flip angle [FA] 75; field of view [FOV] 192 mm; in-plane resolution, 3.0×3.0 mm; 32 slices of 3-mm thickness covering the whole cerebrum) on a 3.0-T magnetic resonance scanner with a standard head coil (Allegra; Siemens, Erlangen, Germany). The interleaved (first slice = bottom) scanning sequence was used. The images were oriented slightly tilted towards the AC-PC line and aligned so that the sample included whole brain. A high-resolutional T1-weighted anatomical brain image of each subject was obtained using an magnetization-prepared rapid gradient-echo sequence (Mugler and Brookeman 1990) with the following parameters: TR = 2500 ms, TE = 4.38 ms, FA = 8°, FOV = 230×230 mm^2, resolution = 0.9×0.9 mm^2.

Image Processing and Statistical Analysis

Imaging processing and statistical analyses were performed using statistical parametric mapping (SPM99; Wellcome Department of Cognitive Neurology, London, UK) (Friston and others 1995; Worsley and Friston 1995) implemented in Matlab (Mathworks, Sherborn, Massachusetts). The first 8 volumes of each fMRI session were discarded because of unsteady magnetization and the remaining 240 volumes per session (480 volumes per subject) were used for analysis. We initially corrected the differences in slice timing within each volume. To remove the motion artifacts, all volumes were then realigned to the first functional image of each session (Friston and others 1994). After being coregistered with a T1-weighted structural volume, they were normalized in the functional scans to the standard stereotaxic space (Montreal Neurological Institute [MNI] template). Then, the images were spatially smoothed using an isotropic Gaussian kernel with a full-width half maximum of 8 mm. Because the event-related (single-event) design was used in this study, specific effects for Aδ- or C-related sensations were estimated for each subject using a general linear model with a regressor waveform assuming the hemodynamic response (HDR) function beginning at the onset of each laser stimulus. To make statistic inferences at the population level, individual data were then summarized and incorporated into a random-effect model. The threshold was set at $P < 0.001$, uncorrected for multiple comparisons (Friston and others 1998).

Results

Following the stimulation of C nociceptors, the bilateral thalamus, bilateral SII, bilateral middle/anterior insular cortex, bilateral posterior portion of the anterior cingulate cortex (pACC), dorsal parts of the anterior portion of the ACC (aACC), and pre-supplementary motor area (pre-SMA) were significantly activated (Fig. 1*a*). The HDRs in the bilateral thalamus, bilateral SII, right (ipsilateral) middle insula, and left pACC peaking at 5 or 7 s following stimulation are shown in Figure 1*b*.

Following Aδ nociceptor stimulation, the bilateral thalamus, bilateral SII, right (ipsilateral) middle insula, and bilateral pACC were significantly activated (Fig. 2*a*). The HDRs in the bilateral thalamus, bilateral SII, right middle insula, and left pACC peaking at 5 or 7 s following stimulation are shown in Figure 2*b*. Overall, the time course of HDRs to the activation of C nociceptors was similar with the time resolution of the present fMRI method. The peak of HDRs in these activated regions showed significant differences between Aδ and C nociceptor stimulation. Activity was significantly stronger following the stimulation of Aδ nociceptors than C nociceptors in the right SII ($P < 0.0001$), left SII ($P < 0.05$), right insular ($P < 0.01$), and left pACC ($P < 0.01$) (paired *t*-test). In contrast, there were no significant differences in the bilateral thalamus ($P = 0.40$ for right thalamus and $P = 0.52$ for left thalamus) (paired *t*-test).

To identify the activity common to and differing between C and Aδ nociceptor stimulation, we used a conjunction analysis in the SPM analysis (Price and Friston 1997; see also Friston and others [2005] and Nichols and others [2005] for the recent discussion on conjunction analysis). The bilateral SII, bilateral thalamus, right (ipsilateral) middle insula, and bilateral Brodmann's area (BA) 24/32 with the majority of activity occurring in the pACC were activated by both C and Aδ nociceptor stimulation (Table 1 and Fig. 3). We then made a direct comparison between C and Aδ nociceptor stimulation. The activation of the right (ipsilateral) BA32/8/6 including dorsal parts of the aACC and pre-SMA and the bilateral anterior insula was significantly greater following C nociceptor stimulation than Aδ nociceptor stimulation ($P < 0.001$) (Table 2 and Fig. 4). By contrast, there were no regions where activity was significantly stronger following the stimulation of Aδ nociceptors than C nociceptors. The activated regions in ACC and pre-SMA are

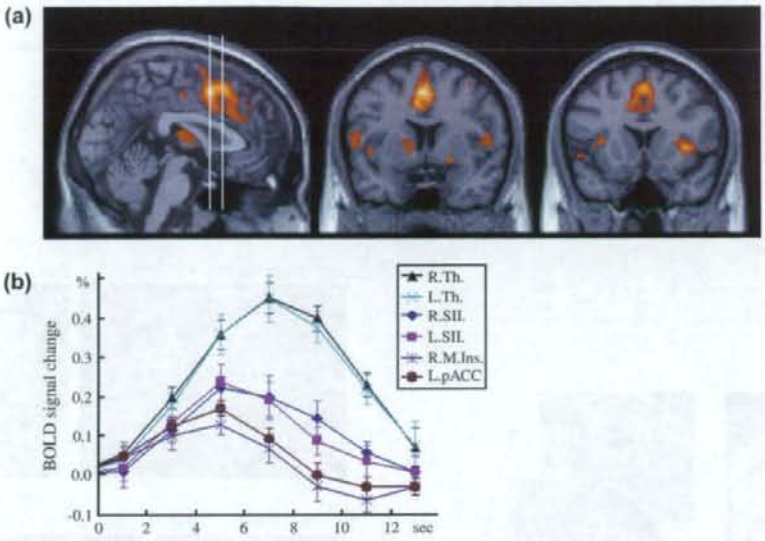

Figure 1. The brain-activated regions and HDRs following C nociceptor stimulation. (*a*) 1 sagittal ($x = 2$, left panel) and 2 coronal ($y = 6$ and 16 for the middle and right panels, respectively) images showing the significant activation to C nociceptor stimulation. Two vertical bars in the left panel indicate the sagittal positions of the 2 coronal planes. (*b*) Time course of HDRs in the activated regions was illustrated. R. = right (ipsilateral to the stimulation), L. = left (contralateral to the stimulation), M. = middle part, Th. = thalamus, SII = secondary somatosensory cortex, Ins. = insula, pACC = posterior portion of the anterior cingulate cortex. Error bars indicate standard deviation.

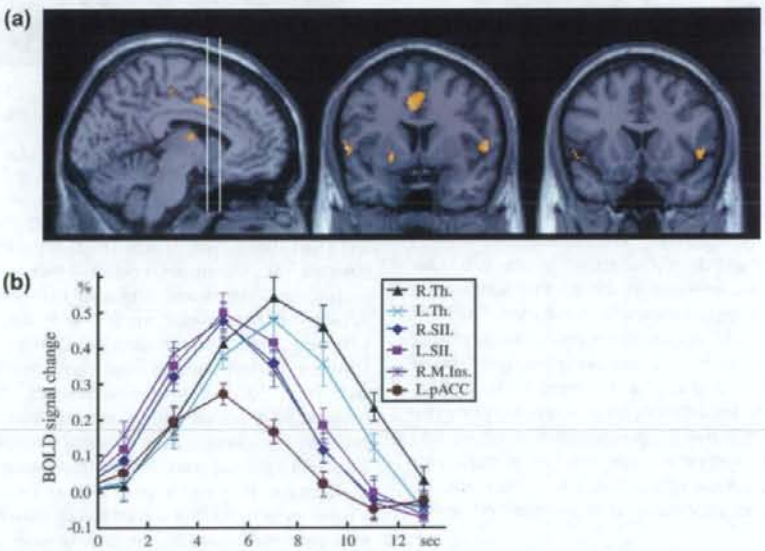

Figure 2. The brain regions activated and HDRs following Aδ nociceptor stimulation. (*a*) 1 sagittal ($x = -6$, left panel) and 2 coronal ($y = 6$ and 16 for the middle and right panels, respectively) images showing the significant activation to Aδ nociceptor stimulation. Two vertical bars in the left panel indicate the sagittal positions of the 2 coronal planes. To make a comparison with Figure 1 easier, the positions of the 2 coronal planes were set identical to those in the previous figure. (*b*) Time course of HDRs in the activated regions was illustrated. R. = right (ipsilateral to the stimulation), L. = left (contralateral to the stimulation), Th. = thalamus, SII = secondary somatosensory cortex, M. Ins. = middle insula, pACC = posterior portion of the anterior cingulate cortex. Error bars indicate standard deviation.

shown in Figure 5. We used the nomenclature based on Devinsky and others (1995) and Kwan and others (2000) to classify the subregions in the ACC, anterior/posterior and dorsal/ventral portion (Buchel and others 2002).

The time course of HDRs in the 2 regions where C nociceptors were activated more than Aδ nociceptors, the right (ipsilateral) BA32/8/6 and bilateral anterior insula, is shown in Figure 6. There were differences following Aδ nociceptor stimulation between these 2 regions. Activated Aδ nociceptors in BA32/8/6 were almost absent, indicating that this region was selectively activated following C nociceptor stimulation and is probably related to second pain. The activity was significantly

Table 1
Coordinates (MNI) of regions activated by both C and Aδ nociceptor stimulation

Brain region (side)	x	y	z	Z-score
Thalamus				
Ipsilateral	8	−6	12	4.14
Contralateral	−12	−4	14	4.02
SII				
Ipsilateral	62	−20	18	4.15
Contralateral	−64	−26	18	4.42
Right middle insula				
Ipsilateral	58	4	4	4.12
BA24/32 (pACC)				
Contralateral	−6	4	42	4.02
Ipsilateral	2	10	48	3.73

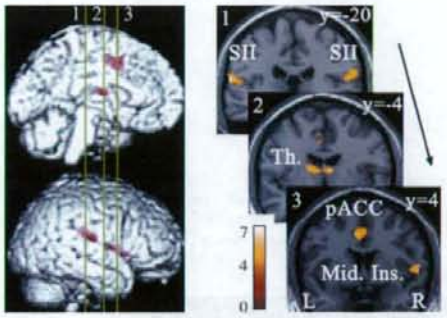

Figure 3. Brain regions commonly activated by C and Aδ nociceptor stimulation. Numbered bars in the left panel indicate locations of coronal slices in the right panel. Activated regions overlaid on an anatomically normalized MRI (MNI template) with their corresponding *y* coordinates (right side). SII = secondary somatosensory cortex, Th. = thalamus, pACC = posterior portion of the anterior cingulate cortex, Mid. Ins. = middle insula. MNI coordinates in Table 1.

Table 2
Coordinates (MNI) of specifically activated regions for C nociceptor stimulation

Brain region (side)	x	y	z	Z-score
BA32/8/6				
Midline, Ipsilateral	6	22	50	4.52
Anterior insula				
Ipsilateral	30	21	3	3.91
Contralateral	−31	25	1	3.56

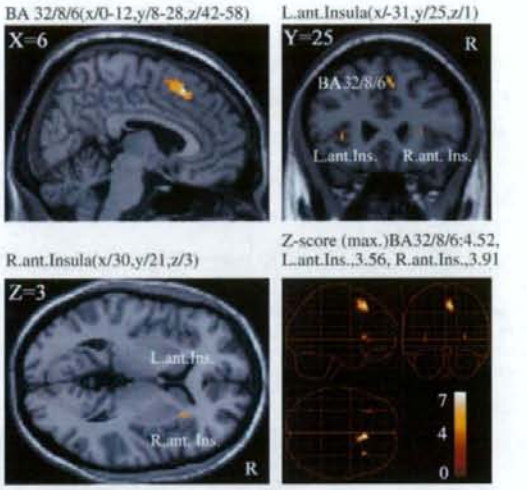

Figure 4. Brain regions differentially activated by C nociceptor stimulation. The activity in these areas was significantly stronger following the stimulation of C nociceptors than Aδ nociceptors ($P < 0.001$, uncorrected) and overlaid on an anatomically normalized MRI (MNI template). BA = Brodmann's area, Ant. Ins. = anterior insula, L. = left, R. = right. MNI coordinates in Table 2.

stronger following the stimulation of C nociceptors than Aδ nociceptors in the time period, 5–9 s, poststimulation ($P < 0.05$) (Fig. 6*a*). However, the bilateral anterior insula was also activated by Aδ nociceptor stimulation, though to a significantly lesser degree than following C nociceptor stimulation. The HDR peaked at 3 s following Aδ nociceptor stimulation, gradually decreased afterward, and then returned to the baseline level at 6 s. By contrast, HDR peaked at 7 s following C nociceptor stimulation, and a significant difference was found between the 2 stimulus conditions at 5 and 7 s poststimulation ($P < 0.05$) (Fig. 6*b*). Therefore, this region is considered to be important for both C and Aδ nociceptor stimulation but is more specifically activated by C nociceptor stimulation, probably related to second pain.

Discussion

In the present fMRI study, we found that the activity in the right (ipsilateral) BA32/8/6, including the dorsal parts of the aACC and pre-SMA, and the bilateral anterior insula was significantly stronger following the stimulation of C nociceptors than Aδ nociceptors, though several regions were activated by both stimuli.

This is the first neuroimaging study to use the phasic stimulation of C nociceptors. As a method for the tonic stimulation of C nociceptors, the injection of capsaicin is commonly used, and a few studies using PET (Andersson and others 1997; Iadarola and others 1998; May and others 1998) and fMRI (Baron and others 1999) reported that the thalamus, striatum, SI, SII, insula cortex, cingulate cortex, prefrontal cortex, and SMA were activated in normal healthy subjects. Activity in the insular cortex was also identified by fMRI following touch stimulation of C fiber tactile afferents in a unique patient lacking large myelinated afferents (Olausson and others 2002). In the present study, the bilateral thalamus, bilateral SII, bilateral middle/anterior insula, bilateral ACC, and pre-SMA were activated, consistent with previous studies using capsaicin-induced pain. By contrast, no activation of the SI or prefrontal cortex was found. Because capsaicin-induced pain is a tonic pain reflecting a mixture of bottom-up and top-down processes and complex pain-coping strategies, the difference in regions activated obtained with the capsaicin injection and our method was probably caused by the difference in the method of stimulation used. However, the finding that the activity in the right (ipsilateral) BA32/8/6, including the dorsal parts of the aACC and pre-SMA, and the bilateral anterior insula, particularly the former, was significantly stronger following stimulation of C nociceptors than Aδ nociceptors was novel.

Following the stimulation of Aδ nociceptors in the present study, the bilateral thalamus, bilateral SII, right (ipsilateral) middle insula, and pACC were activated, consistent with recent neuroimaging studies using PET and fMRI following stimulation with CO_2 or a Tm:YAG laser. However, a German group (Bingel

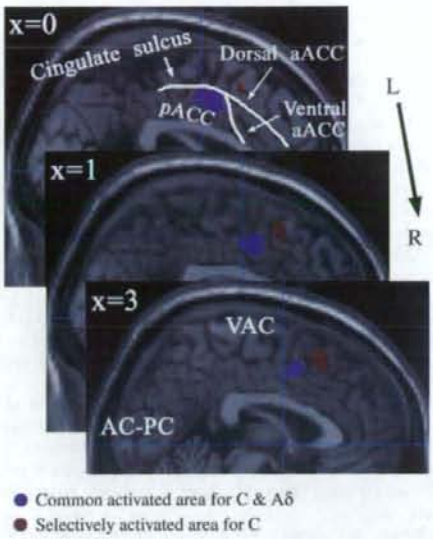

Figure 5. Activations in the ACC and pre-SMA overlaid on an anatomically normalized MRI (MNI template). These are shown from left (top part of the image) to right (bottom part of the image) with their corresponding MNI template *x* coordinates. The blue vertical line indicates the line through the anterior commissure (VAC). aACC = anterior portion of the anterior cingulate cortex, pACC = posterior portion of the anterior cingulate cortex.

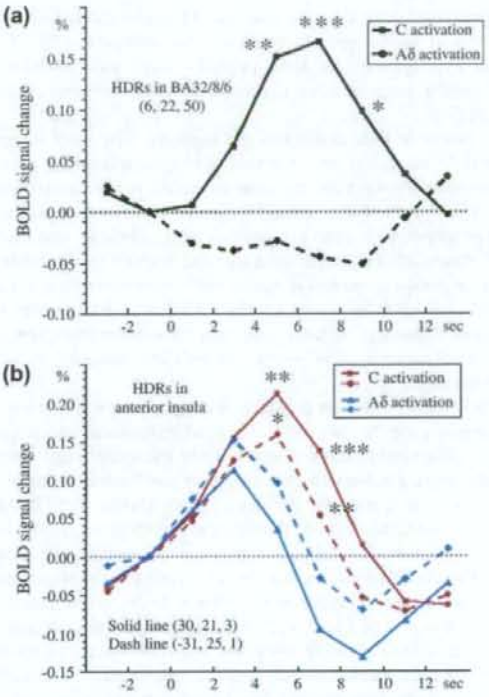

Figure 6. Time course of the HDRs in the BA32/8/6 and bilateral anterior insula following stimulation of C and Aδ nociceptors. (*a*) In the right (ipsilateral) BA32/8/6, the HDR following Aδ nociceptor stimulation was almost below the baseline, whereas that following C nociceptor stimulation was very large. The difference between them, 5–9 s, after stimulation was significant. (*b*) In the bilateral anterior insula cortex (solid/dashed line = right/left anterior insula), the HDR following Aδ nociceptor stimulation peaked at 3 s, rapidly decreased thereafter, and had returned to the baseline level at 6 s. By contrast, the HDR following C nociceptor stimulation was large for a long period, peaking at 5 s, and the difference between 5 and 7 s after stimulation was significant (the paired *t*-test was calculated from red solid to blue solid lines and red dashed to blue dashed lines) (*P < 0.05, **P < 0.01, ***P < 0.001).

and others 2002; Bornhovd and others 2002; Buchel and others 2002; Bingel, Glascher, and others 2004; Bingel, Lorenz, and others 2004) reported that many regions involving the SI, hippocampus, amygdala, prefrontal cortex, SMA, motor cortex, putamen, red nucleus, brainstem, and cerebellum were also activated in addition to the regions identified in the present study. We consider the difference between their findings and ours to be mainly due to the method of analysis because the German group used a fix-effect model whereas we used a random-effect model during the group analysis with uncorrected values and set the threshold at $P < 0.001$. In any case, the areas important for pain perception may be those where both groups identified activity.

We found activity in the pACC following the stimulation of both Aδ and C nociceptors and in the dorsal part of the aACC following the stimulation of only C nociceptors. Hutchison and others (1999) detected activity in the pACC following painful thermal stimulation using single-neuron recordings in conscious subjects. Buchel and others (2002) demonstrated that the pACC is associated with pain intensity, and dorsal parts of the aACC are associated with cognitive processing like attention and working memory and stimulus awareness related to pain. In addition, the dorsal ACC also plays important roles in cognition, motor control, and emotional processing (Bush and others 2002). Therefore, our findings indicate that the activation of the dorsal parts of the aACC through the stimulation of C nociceptors, probably related to second pain, is closely related to the cognitive aspect of pain as compared with the stimulation of the Aδ nociceptors (first pain). Recently, Bush and others (2000) and Vogt and others (2003) reviewed anatomical and physiological findings of cingulate cortex. Bush and others (2000) separated ACC into 2 parts by their roles; the more anterior part plays a main role for emotional tasks and the posterior part does so for tasks. The activated region found in the present study was consistent with the emotional region reported by them; Vogt and others (2003) also separated the cingulate cortex into 3 parts: noxious thermal region, emotional region, and nonemotional region, and the activated region found in the present study was consistent with the noxious region and emotional region reported by them, mainly the former.

Activation in the SMA has been reported following various noxious stimulations such as heat (Coghill and others 1994; Kwan and others 2000), cooling (Kwan and others 2000), CO_2 laser (Svensson and others 1997), ethanol injection (Hsieh and others 1996), and thermal grill (Craig and others 1996). Kwan and others (2000) reported fMRI study of the activation of the ACC and surrounding medial wall using innocuous and noxious thermal-related stimuli and motor-related stimuli and noxious stimuli activated mainly aACC, pACC, and SMA proper and modestly pre-SMA too. Picard and Strick (2001) reviewed imaging studies of the premotor cortex and concluded that it might be more appropriate to consider the pre-SMA as a functional component of the prefrontal cortex rather than

as a premotor area. Because the dorsal parts of the aACC is also considered as a cognitive region (Bush and others 2002), it seems appropriate that both pre-SMA and caudal division of ACC play a main role for cognitive function for second pain perception.

Studies of lesions in animals and humans, functional imaging related to attention and emotion, and opioid-binding experiments have shown that the anterior insula is coactivated with the ACC to reflect active modulation by the affective agent of pain perception (Peyron and others 2000; Schnizler and Ploner 2000; Craig 2002). Our finding that the activity in the bilateral anterior insular cortex was significantly stronger following the stimulation of C nociceptors than Aδ nociceptors, which is probably related to second pain, reflects greater attention and behavioral motivation as compared with first pain (Aδ nociceptor stimulation).

It is obvious that first pain and second pain are experienced differently probably because of several anatomical and physiological differences. In the dorsal horn of the spinal cord, lamina II is the input nucleus for C nociceptors and laminae I and V are major output nuclei for Aδ nociceptors (Willis 1985). Since Melzack and Casey (1968) divided the nociceptive system into lateral (sensory-discriminative aspects of pain) and medial (affective-motivational aspects of pain) systems, the supraspinal parts of the nociceptive system have been investigated by a large number of functional imaging studies (see review by Treede and others 1999). However, the difference of activated brain regions between Aδ and C nociceptor stimulation remained to be investigated. We found that the activity in the bilateral insula and dorsal parts of the ACC and pre-SMA was significantly greater following stimulation of C nociceptors than Aδ nociceptors in this study. These findings may indicate that the C nociceptors play a more important role in the medial system, whereas the Aδ nociceptors play a more important role in the lateral system, the sensory–discriminative aspects of pain.

In conclusion, our findings seem to suggest that the differences in brain activity between first and second pain perception probably reflect distinct biological functions of the 2 sensations as found in this study. It is considered that first pain aims at achieving relative safety from the source of injury, whereas second pain, with its strong affective component, attracts longer lasting attention and initiates behavioral responses to limit further injury and optimize recovery (Wall 1979). Therefore, dorsal parts of the aACC, pre-SMA, and anterior insular cortex should play some role in the perception of second pain.

Notes

This study was supported by Japan Space Forum, and Grant-in-Aid for Scientific Research on Priority Areas—Higher-Order Brain Functions—from The Ministry of Education, Culture, Sports, Science and Technology, Japan.

Address correspondence to Ryusuke Kakigi, MD, PhD, Department of Integrative Physiology, National Institute for Physiological Sciences, Myodaiji, Okazaki 444-8585, Japan. Email: kakigi@nips.ac.jp.

Funding to pay the Open Access publication charges for this article was provided by the Ministry of Education, Culture, Sports, Science and Technology, Japan, and by the Japanese Science and Technology Agency.

References

Andersson JL, Lilja A, Hartvig P, Langstrom B, Gordh T, Handwerker H, Torebjork E. 1997. Somatotopic organization along the central sulcus, for pain localization in humans, as revealed by positron emission tomography. Exp Brain Res 117:192–199.

Baron R, Baron Y, Disbrow E, Roberts TP. 1999. Brain processing of capsaicin-induced secondary hyperalgesia: a functional MRI study. Neurology 11:548–557.

Bingel U, Glascher J, Weiller C, Buchel C. 2004. Somatotopic representation of nociceptive information in the putamen: an event-related fMRI study. Cereb Cortex 14:1340–1345.

Bingel U, Lorenz J, Glauche V, Knab R, Glascher J, Weiller C, Buchel C. 2004. Somatotopic organization of human somatosensory cortices for pain: a single trial fMRI study. Neuroimage 23:224–232.

Bingel U, Quante M, Knab R, Bromm B, Weiller C, Buchel C. 2002. Subcortical structures involved in pain processing: evidence from single-trial fMRI. Pain 99:313–321.

Bornhovd K, Quante M, Glauche V, Bromm B, Weiller C, Buchel C. 2002. Painful stimuli evoke different stimulus-response functions in the amygdala, prefrontal, insula and somatosensory cortex: a single-trial fMRI study. Brain 125:1326–1336.

Bragard D, Chen CAN, Plaghki L. 1996. Direct isolation of ultra-late (C-fibre) evoked brain potentials by CO_2 laser stimulation of tiny cutaneous surface areas in man. Neurosci Lett 209:81–84.

Bromm B, Treede RD. 1984. Nerve fibre discharges, cerebral potentials and sensations induced by CO_2 laser stimulation. Hum Neurobiol 3:33–40.

Buchel C, Bornhovd K, Quante M, Glauche V, Bromm B, Weiller C. 2002. Dissociable neural responses related to pain intensity, stimulus intensity, and stimulus awareness within the anterior cingulate cortex: a parametric single-trial laser functional magnetic resonance imaging study. J Neurosci 22:970–976.

Bush G, Luu P, Posner MI. 2000. Cognitive and emotional influences in anterior cingulate cortex. Trends Cogn Sci 4:215–222.

Bush G, Vogt BA, Holmes J, Dale AM, Greve D, Jenike MA, Rosen BR. 2002. Dorsal anterior cingulate cortex: a role in reward-based decision making. Proc Natl Acad Sci USA 99:523–528.

Coghill RC, Talbot JD, Evans AC, Meyer E, Gjedde A, Bushnell MC, Duncan GH. 1994. Distributed processing of pain and vibration by the human brain. J Neurosci 14:4095–4108.

Craig AD. 2002. How do you feel? Interoception: the sense of the physiological condition of the body. Nat Rev Neurosci 3:655–666.

Craig AD, Reiman EM, Evans A, Bushnell MC. 1996. Functional imaging of an illusion of pain. Nature 384:258–260.

Devinsky O, Morrell MJ, Vogt BA. 1995. Contributions of anterior cingulate cortex to behaviour. Brain 118:279–306.

Friston KJ, Fletcher P, Josephs O, Holmes A, Rugg MD, Turner R. 1998. Event-related fMRI: characterizing differential responses. Neuroimage 7:30–40.

Friston KJ, Holmes AP, Poline JB, Grasby PJ, Williams SC, Frackowiak RS, Turner R. 1995. Analysis of fMRI time-series revisited. Neuroimage 1:45–53.

Friston KJ, Holmes AP, Worsley KJ, Poline JP, Frith, CD, Frackowiak RSJ. 1994. Statistical parametric maps in functional imaging: a general linear approach. Hum Brain Mapp 2:189–210.

Friston KJ, Penny WD, Glaser DE. 2005. Conjunction revisited. Neuroimage 25:661–667.

Holzer P. 1991. Capsaicin: cellular targets, mechanisms of action, and selectivity for thin sensory neurons. Pharmacol Rev 43:143–201.

Hsieh J-C, Ståhle-Bäckdahl M, Hägermark O, Stone-Elander S, Rosenquist G, Ingvar M. 1996. Traumatic nociceptive pain activates the hypothalamus and the periaqueductal gray: a positron emission tomography study. Pain 64:303–314.

Hutchison WD, Davis KD, Lozano AM, Tasker RR, Dostrovsky JO. 1999. Pain-related neurons in the human cingulate cortex. Nat Neurosci 2:403–405.

Iadarola MJ, Berman KF, Zeffiro TA, Byas-Smith MG, Gracely RH, Max MB, Bennett GJ. 1998. Neural activation during acute capsaicin-evoked pain and allodynia assessed with PET. Brain 121:931–947.

Kakigi R, Tran TD, Qiu Y, Wang X, Nguyen TB, Inui K, Watanabe S, Hoshiyama M. 2003. Cerebral responses following stimulation of unmyelinated C-fibers in humans: Electro- and magneto-encephalographic study. Neurosci Res 45:255–275.

Kwan CL, Crawley AP, Mikulis DJ, Davis KD. 2000. An fMRI study of the anterior cingulate cortex and surrounding medial wall activations evoked by noxious cutaneous heat and cold stimuli. Pain 85:359–374.

Mauguiere F, Frot M, Peyron R, Garcia-Larrea L, Laurent B, Michel D. 1999. The role of parietal opercular and insular cortex in pain sensation in humans: data from PET activation studies and intracortical recordings of CO_2 laser evoked potentials (LEPs). Electroencephalogr Clin Neurophysiol Suppl 49:255–260.

May A, Kaube H, Buchel C, Eichten C, Rijntjes M, Juptner M, Weiller C, Diener HC. 1998. Experimental cranial pain elicited by capsaicin: a PET study. Pain 74:61–66.

Melzack R, Casey KL. 1968. Sensory, motivational, and central control determinations of pain. A new conceptional model. In: Kenshalo DR, editor. The Skin Senses. Springfield, IL: Charles C. Thomas. p 423–443.

Mendell LM, Wall PD. 1965. Responses of single dorsal cord cells to peripheral cutaneous unmyelinated fibres. Nature 3:97–99.

Mor J, Carmon A. 1975. Laser emitted radiant heat for pain research. Pain 1:233–237.

Mugler JP, Brookeman JR. 1990. Three-dimensional magnetization-prepared rapid gradient-echo imaging (3D MP RAGE). Magn Reson Med 15:152–157.

Nichols T, Brett M, Andersson J, Wager T, Poline JB. 2005. Valid conjunction inference with the minimum statistic. Neuroimage 25:653–660.

Ochoa J, Torebjork E. 1989. Sensations evoked by intraneural microstimulation of C nociceptor fibres in human skin nerves. J Physiol 415:583–599.

Olausson H, Lamarre Y, Backlund H, Morin C, Wallin BG, Starck G, Ekholm S, Strigo I, Worsley K, Vallbo AB, Bushnell MC. 2002. Unmyelinated tactile afferents signal touch and project to insular cortex. Nat Neurosci 9:900–904.

Opsommer E, Masquelier E, Plaghki L. 1999. Determination of nerve conduction velocity of C-fibers in humans from thermal thresholds to contact heat (thermode) and from evoked brain potentials to radiant heat (CO_2 laser). Neurophysiol Clin 29:411–422.

Peyron R, Laurent B, Garcia-Larrea L. 2000. Functional imaging of brain responses to pain. A review and meta-analysis. Neurophysiol Clin 30:263–288.

Picard N, Strick PL. 2001. Imaging the premotor areas. Curr Opin Neurobiol 11:663–672.

Plaghki L, Mouraux A. 2003. How do we selectively activate skin nociceptors with a high power infrared laser? Physiology and biophysics of laser stimulation. Neurophysiol Clin 33:269–277.

Ploner M, Gross J, Timmermann L, Schnitzler A. 2002. Cortical representation of first and second pain sensation in humans. Proc Natl Acad Sci USA 17:12444–12448.

Price CJ, Friston KJ. 1997. Cognitive conjunction: a new approach to brain activation experiments. Neuroimage 5:261–270.

Price DD, Hu JW, Dubner R, Gracely RH. 1977. Peripheral suppression of first pain and central summation of second pain evoked by noxious heat pulses. Pain 3:57–68.

Qiu Y, Fu Q, Wang X, Tran TD, Inui K, Iwase S, Kakigi R. 2003. Microneurographic study of C fiber discharges induced by CO_2 laser stimulation in humans. Neurosci Lett 15:25–28.

Qiu Y, Inui K, Wang X, Nguyen BT, Tran TD, Kakigi R. 2004. Effects of distraction on magnetoencephalographic responses ascending through C-fibers in humans. Clin Neurophysiol 115:636–646.

Qiu Y, Inui K, Wang X, Tran TD, Kakigi R. 2001. Conduction velocity of the spinothalamic tract in humans as assessed by CO_2 laser stimulation of C-fibers. Neurosci Lett 311:181–184.

Qiu Y, Inui K, Wang X, Tran TD, Kakigi R. 2002. Effects of attention, distraction and sleep on CO_2 laser evoked potentials related to C-fibers in human. Clin Neurophysiol 113:1579–1585.

Sawamoto N, Honda M, Okada T, Hanakawa T, Kanda M, Fukuyama H, Konishi J, Shibasaki H. 2000. Expectation of pain enhances responses to nonpainful somatosensory stimulation in the anterior cingulate cortex and parietal operculum/posterior insula: an event-related functional magnetic resonance imaging study. J Neurosci 20:7438–7445.

Schmidt RF, Schaible HG, Messlinger K, Heppelmann B, Hanesch U, Pawlak M. 1994. Silent and active nociceptors: structure, functions, and clinical implications. In: Gebhart GF, Hammond DL, Jensen TS, editors. Proceedings of the 7th World Congress on Pain. Seattle, WA: IASP Press. p 213–250.

Schnitzler A, Ploner M. 2000. Neurophysiology and functional neuroanatomy of pain perception. J Clin Neurophysiol 17:592–603.

Svensson P, Minoshima S, Beydoun A, Morrow TJ, Casey KL. 1997. Cerebral processing of acute skin and muscle pain in humans. J Neurophysiol 78:450–460.

Szallasi A. 1994. The vanilloid (capsaicin) receptor: receptor types and species differences. Gen Pharmacol 25:223–243.

Tran TD, Inui K, Hoshiyama M, Lam K, Kakigi R. 2003. Conduction velocity of the spinothalamic tract following CO_2 laser stimulation of C-fiber in humans. Pain 95:125–131.

Tran TD, Inui K, Hoshiyama M, Lam K, Qiu Y, Kakigi R. 2002. Cerebral activation by the signals ascending through unmyelinated C-fibers in humans: a magnetoencephalographic study. Neuroscience 113: 375–386.

Tran TD, Lam K, Hoshiyama M, Kakigi R. 2001. A new method for measuring the conduction velocities of Aβ-, Aδ- and C-fibers following electric and CO_2 laser stimulation in humans. Neurosci Lett 301:187–190.

Treede RD, Kenshalo DR, Gracely RH, Jones AK. 1999. The cortical representation of pain. Pain 79:105–111.

Treede RD, Meyer RA, Lesser RP. 1994. Similarity of threshold temperatures for first pain sensation, laser-evoked potentials, and nociceptor activation. In: Gebhart GF, Hammond DL, Jensen TS, editors. Proceedings of the 7th World Congress on Pain. Seattle, WA: IASP Press. p 857–865.

Vogt BA, Berger GR, Derbyshire SWG. 2003. Structural and functional dichotomy of human midcingulate cortex. Eur J Neurosci 18: 3134–3144.

Wall PD. 1979. On the relation of injury to pain. The John J. Bonica lecture. Pain 6:253–264.

Willis WD. 1985. The Pain System. Basel, Switzerland: Karger.

Worsley KJ, Friston, KJ. 1995. Analysis of fMRI time-series revisited—again. Neuroimage 2:173–181.

Xu X, Fukuyama H, Yazawa S, Mima T, Hanakawa T, Magata Y, Kanda M, Fujiwara N, Shindo K, Nagamine T, Shibasaki H. 1997. Functional localization of pain perception in the human brain studied by PET. Neuroreport 8:555–559.

Neuromodulation

Technology at the Neural Interface

VOLUME XI • NUMBER 1 • JANUARY 2008

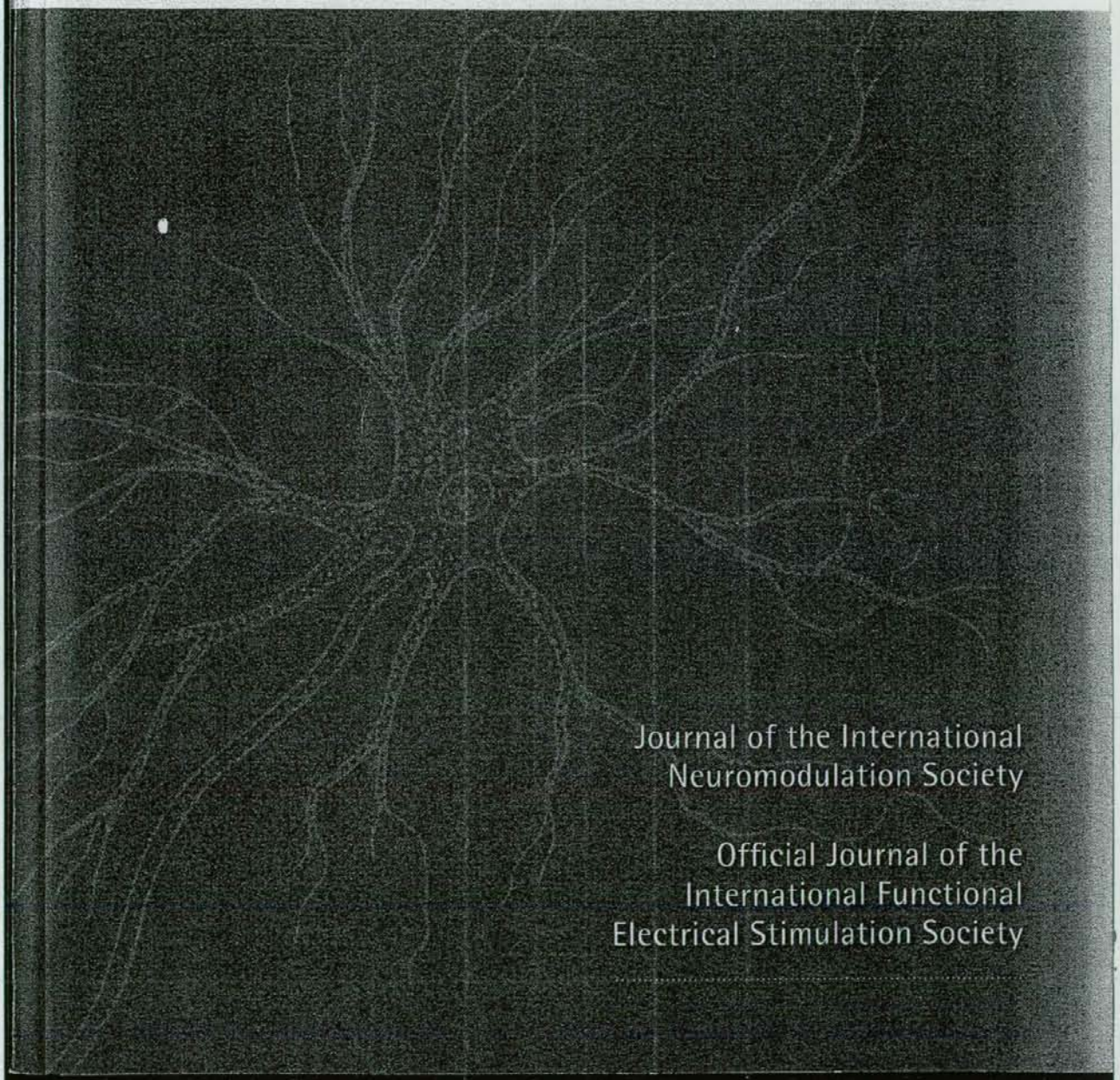

Journal of the International Neuromodulation Society

Official Journal of the International Functional Electrical Stimulation Society

NEUROMODULATION: TECHNOLOGY AT THE NEURAL INTERFACE

Volume 11 • Number 1 • 2008
http://www.blackwell-synergy.com/loi/ner

ORIGINAL ARTICLE

Multiple-Cell Spike Density and Neural Noise Level Analysis by Semimicroelectrode Recording for Identification of the Subthalamic Nucleus During Surgery for Parkinson's Disease

Toshikazu Kano, MD, PhD[1,2] • Yoichi Katayama, MD, PhD[1,2] • Kazutaka Kobayashi, MD, PhD[1,2] • Masahiko Kasai, MD, PhD[1] • Hideki Oshima, MD, PhD[1] • Chikashi Fukaya, MD, PhD[1,2] • Takamitsu Yamamoto, MD, PhD[1,2]

Department of Neurological Surgery, and Division of Applied System Neuroscience, Department of Advanced Medical Science, Nihon University School of Medicine, Tokyo, Japan

ABSTRACT

Objective. For targeting the subthalamic nucleus (STN), we attempted to quantify the changes in multiple cell activities by computing the neural noise level and multiple-cell spike density (MSD). **Methods.** We analyzed the neural noise level and MSD by stepwise recording at every 0.25-mm increment during the final tracking in 90 sides of 45 patients with Parkinson's disease. The MSD was analyzed with cut-off levels ranging from 1.2- to 2.0-fold the neural noise level in the internal capsule or zona incerta in each trajectory. **Results.** The dorsal boundary of the STN was identified from an increase in the neural noise ratio in all sides. The ventral boundary was identifiable, however, from a decrease in the neural noise ratio in only 70 sides (78%). In contrast, both the dorsal and ventral boundaries were clearly identified from an increase and a decrease in the MSD, respectively, in all of the 90 sides. **Conclusion.** MSD analysis by semimicroelectrode recording represents a useful, practical, and apparently reliable means for identifying the boundaries of the STN.

KEY WORDS: *Deep brain stimulation, Parkinson's disease, semimicroelectrode, subthalamic nucleus.*

Introduction

Deep brain stimulation (DBS) of the subthalamic nucleus (STN) affords great benefits to the daily activity of patients with advanced Parkinson's disease (PD) (1–4). Most recent reports have placed emphasis on the microelectrode recording of single cell activity to refine the anatomical targeting of the STN during surgery (5–11). When the electrode has passed through the dorsal boundary of the STN, densely distributed cells characterized by irregular discharges are encountered (10,12,13). Detection of cells characterized by rapid and tonic discharges indicates that the electrode has passed through the dorsal boundary of the STN (14).

The ventral boundary of the STN, however, is sometimes unclear (10). This is because the cells in the STN

Submitted: July 10, 2007; accepted: September 11, 2007.
Address correspondence and reprint requests to: Yoichi Katayama, MD, PhD, Department of Neurological Surgery, Nihon University School of Medicine, 30-1 Ohyaguchi Kamimachi, Itabashi-ku, Tokyo 173-8610, JAPAN. Email: ykatayam@med.nihon-u.ac.jp

show several different discharge patterns (12,14). Multiple sampling of single cell activities is useful through changing the location of the electrode tip to determine whether or not the electrode has passed through the ventral boundary of the STN and entered the small band of white matter and pars reticulata of the substantia nigra (SNr).

We have been employing semimicroelectrode recording (1,15–18) for many years in an attempt to refine anatomical targeting. The semimicroelectrode can detect electrical events arising from a relatively wide area. This method results in stable recordings of spikes and neural noise generated by multiple cells at any location of the electrode tip, and enables stepwise recording with predetermined intervals. In addition, a relatively blunt tip of the semimicroelectrode, as compared to a sharp tip of the microelectrode, may be associated with a lower risk of hemorrhagic complications (14,19).

Semimicroelectrode recording of multiple cell activities as a whole reveals robust changes at the dorsal and ventral boundaries of the STN, and, therefore, appears to be more practical and time-saving. Little has yet been reported, however, concerning the standardization of such a technique. We attempted in the present study to quantify the changes in multiple cell activities by computing the multiple-cell spike density (MSD).

Materials and Methods

Patient Population

We analyzed data from intraoperative semimicroelectrode recordings in 45 patients, including 23 men and 22 women ranging in age from 42 to 80 (mean = 65), who underwent single-stage surgery for bilateral STN-DBS. These patients were diagnosed as having idiopathic PD and demonstrated past evidence of a good response to levodopa, but were disabled by severe motor symptoms despite receiving medications at a tolerable dose and schedule. The patients' Hoehn and Yahr stage with medication was within the range from stage III–V during the off-period, and stage II–IV during the on-period. The patients and their families gave informed consent for STN-DBS with intraoperative semimicroelectrode recording to be performed. Patients continued best medication on the day before the DBS operation and even on the morning of the day of the DBS operation. The clinical characteristics and demographic data for all 45 patients are summarized in Table 1.

TABLE 1. Clinical Characteristics and Demographic Data for All 45 Patients

	Characteristics
No. of patients	45
Male/female ratio	23:22
Age (years)[a]	
At diagnosis	55.3 ± 8.2
At surgery	65.0 ± 7.5
LED (mg/day)	627.0 ± 305.9
UPDRS parts 1–4[a]	
On period	39.3 ± 18.0
Off period	69.4 ± 20.9
UPDRS part 3[a]	
On period	21.7 ± 12.6
Off period	37.9 ± 14.5

[a]Data are expressed as the means ± SD.
LED, levodopa equivalent dose; UPDRS, Unified Parkinson's Disease Rating Scale.

Surgical Procedures

A Leksell Series G head frame (Elekta Instrument AB, Stockholm, Sweden) was fixed to the skull. Magnetic resonance imaging (MRI; 1.5-tesla unit; Siemens Magnetom Vision®, Siemens AG, Erlangen, Germany) was carried out at a 1-mm slice thickness, and the anterior commissure and posterior commissure were identified with specialized software (Leksell SurgiPlan®, Elekta Instrument AB).

In an attempt to minimize cerebrospinal fluid leakage and, consequently, intraoperative brain shift, the head was elevated to approximately 30 degrees from the horizontal plane and the burr hole was made 30–35 mm anterior to the coronal suture and 20–25 mm lateral to the midline (17,20,21). The STN was then approached from the burr hole at an angle of 40–50 degrees to the horizontal plane parallel to the anterior commissure–posterior commissure line and 0–12.5 degrees to the sagittal plane. The tentative target was placed at the posteroventral boundary of the STN in such a way that the trajectory passed through the center of the STN. The trajectory was visualized three-dimensionally on MRI, onto which a digitized version of the Schaltenbrand-Wahren atlas (AtlasSpace®, Elekta Instrument AB) was superimposed (Fig. 1).

A DBS quadripolar electrode (model 3387; Medtronic Inc., Minneapolis, MN, USA) was placed through the frontal burr hole into the STN. Contact point 0 was placed in the posteroventral boundary of the STN, contact points 1 and 2 were placed within the STN, and contact point 3 was placed at the H fields of Forel or zona incerta (ZI) located just above the STN. Immediately after completion of the stereotactic operation, we undertook MRI again under conditions where the stereotactic frame was fixed to the skull, and the locations of each contact point of the DBS electrode were confirmed. The mean coordinates of the center of the most distal simulation point, as evaluated by postoperative MRI, were 11.0 mm lateral, 4.5 mm posterior, and 5.2 mm inferior to the mid-commissural point. DBS electrodes were implanted bilaterally as single-stage surgery in all patients. No hemorrhagic complications were encountered in this series of patients.

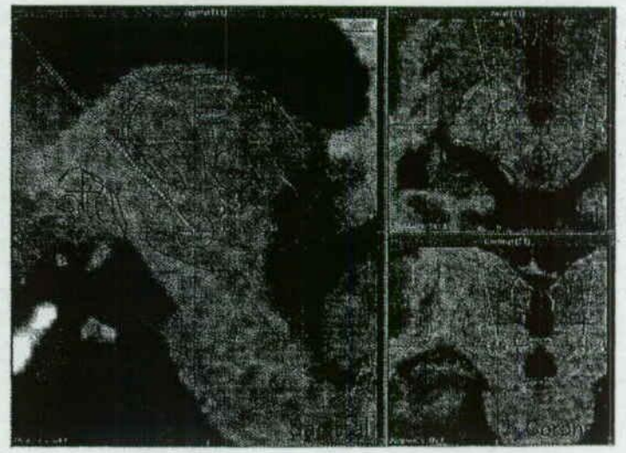

FIGURE 1. Simulation of the trajectory of the semimicroelectrode for targeting the STN. The trajectory is visualized three-dimensionally on MRI, onto which a digitized version of the Schaltenbrand–Wahren atlas adjusted to the size of each brain is superimposed. *Red crosses* indicate the positions of the anterior commissure and posterior commissure projected to the sagittal, axial, and coronal planes of the tentative target. *White dotted lines* indicate the simulated trajectory of the semimicroelectrode. *The green cross within a circle* is the tentative target, which is located at the posteroventral boundary of the STN. The simulated trajectory passes through the H2 fields of Forel (*yellow dotted triangle*) and the STN (*green dotted oval ring*). *The red dotted area* just below the tentative target is the SNr. MRI, magnetic resonance imaging; SNr, pars reticulata of the substantia nigra; STN, subthalamic nucleus.

Semimicroelectrode Recording

Neural activities were recorded with a pencil-shaped bipolar concentric type semimicroelectrode (Unique Medical Co., Tokyo, Japan). The diameter of the exposed tip was approximately 0.1 mm, and the interpolar distance was 0.5 mm with an electrical resistance of 0.2 mΩ at 1000 Hz. The catheter needle (Leksell Stereotactic System, Elekta Instrument AB) with an outer diameter of 2.1 mm and inner diameter of 1.5 mm was first inserted and advanced to a point 10 mm above the tentative target, and the semimicroelectrode with a diameter of 1.0 mm was passed through the inside of the catheter needle.

Tracking with the semimicroelectrode was performed targeting the posteroventral boundary of the STN. The tip of the semimicroelectrode was advanced in consecutive 0.25-mm increments from a depth of 10 mm above the tentative target employing a hydraulic microdrive (Narishige Co., Tokyo, Japan). Recording first yielded the ventral anterior thalamic nucleus or the internal capsule (IC), and this was always followed by the ZI and H fields of Forel before entering the STN. In addition, the semimicroelectrode was further advanced 3 mm from the tentative target to confirm the border between the STN and the SNr. Signals were amplified, filtered (300 Hz to 10 kHz), displayed on an oscilloscope, played on an audio monitor, and stored in a data recorder. When the semimicroelectrode recording in the initial track failed to detect neural activity consistent with the STN at a length (distance from dorsal to ventral boundary) greater than 4 mm, a second tracking was made. We moved the tentative target depending on the characteristics of the recorded neural activity and the position of the semimicroelectrode verified from an intraoperative X-ray film taken after the semimicroelectrode recording.

Analysis of Neural Noise Level and Multiple-Cell Spike Density

The electrical events recorded by a semimicroelectrode include spikes with variable amplitudes arising from multiple cells as well as neural noise, ie, fluctuations of field potentials generated by various neural elements. Large amplitude spikes could be separated from neural noise by setting an appropriate cut-off level of amplitude. It is not always possible, however, to separate small- or medium-sized spikes from sharp compound waves, which are contained in the neural noise. Therefore, we computed the density of spikes as well as sharp compound waves together, as the MSD, counting their occurrence at various cut-off levels.

In the final tracking by semimicroelectrode recording, we determined the neural noise level along the trajectory (Fig. 2A). The neural noise level was defined as the lowest cut-off level at which the neural noise was separated from larger amplitude spikes. The MSD at a given recording

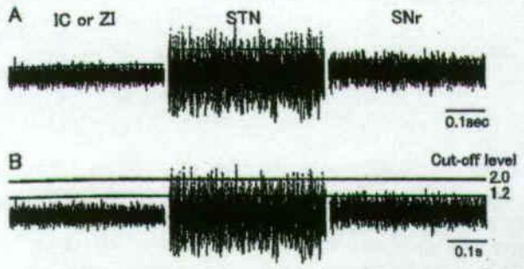

FIGURE 2. (A) Neural noise levels in the IC, STN and SNr. The neural noise level was defined as the lowest cut-off level at which the neural noise was separated from larger amplitude spikes. (B) Cut-off levels for analyzing the MSD were set in the range from 1.2- to 2.0-fold the neural noise level recorded at the IC or ZI. When the electrode entered the STN, the neural noise level was raised more than twofold the level recorded at the IC or ZI. IC, Internal capsule; MSD, multiple-cell spike density; SNr, pars reticulata of the substantia nigra; STN, subthalamic nucleus; ZI, zona incerta.

site was analyzed with cut-off levels ranging from 1.2- to 2.0-fold the neural noise level in the IC or ZI (Fig. 2B), and we examined to find the best cut-off level in each trajectory. Because, as the electrode enters the STN, the neural noise level is raised more than 2.0-fold the level in the IC or ZI (see Results), the MSD within the STN reflects both spikes and sharp compound waves, although spikes are predominantly represented at higher cut-off levels. For identification of the dorsal and ventral boundaries of the STN, the differences in neural noise level and MSD were compared at each 0.25-mm increment of the electrode. The neural noise level and MSD recorded at every 0.25-mm increment were averaged in each structure, and used for comparisons between the IC or ZI, the STN, and the SNr.

The data are expressed as the means ± standard deviation. For statistical analysis, the Mann–Whitney *U*-test was used for comparisons of the MSD and neural noise level, and the Kruskal–Wallis *H*-test for comparisons of the MSD within the STN. If the probability value was less than 0.05, the difference was considered to be significant. The present study was approved by the institutional committee for clinical research on humans.

Results

Changes in Neural Noise Level Along the Trajectory

The neural noise level clearly increased when the electrode crossed the dorsal boundary of the STN, and decreased when the electrode passed through the ventral boundary of the STN and entered the SNr (Fig. 3). The neural noise ratio (neural noise level in each structure/neural noise level in the IC or ZI) was clearly higher in the STN (2.52 ± 0.73) as compared to that of the SNr (1.43 ± 0.35; $p < 0.0001$, $N = 90$; Fig. 4).

The dorsal boundary of the STN was definitely identified from an increase in neural noise ratio during the final tracking in all of the 90 sides. The ventral boundary of the STN was identifiable, however, from a decrease in neural noise ratio during the final tracking in only 70 (78%) of the 90 sides. In the remaining 20 sides (22%), the border between the STN and SNr was unclear (Fig. 5A). In these cases, the neural noise ratio began to decrease in the posteroventral part of the STN before the electrode passed through the ventral boundary of the STN as presumed by MSD analysis (see below).

FIGURE 3. Changes in multiple cell activities along the trajectory (*dotted line*) passing through the subthalamic nucleus (STN). The recording, which was initiated at 10 mm above the tentative target, first yielded the internal capsule, followed by the zona incerta (ZI) and H2 field of Forel (H2), STN, and substantia nigra (SNr). The multiple cell activities increased markedly when the electrode entered the STN, and decreased when the electrode passed through the ventral boundary of the STN. Numbers indicate the distance (mm) from the tentative target (*dotted arrow*) set at the posteroventral boundary of the STN.

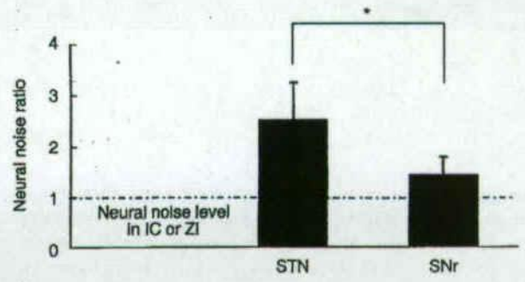

FIGURE 4. Comparison of neural noise levels along the trajectory passing through the STN. Data are expressed as the neural noise ratio (neural noise level in each structure/neural noise level in the IC or ZI), $*p < 0.0001$. IC, internal capsule; STN, subthalamic nucleus; ZI, zona incerta.

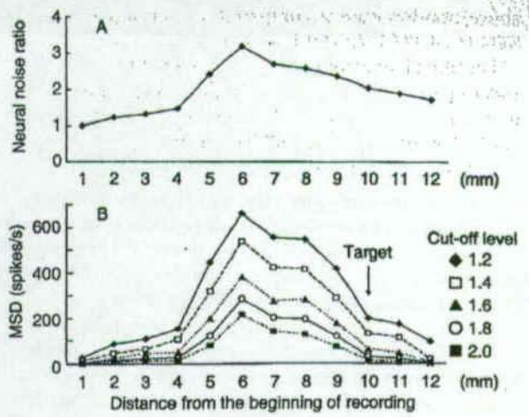

FIGURE 5. (A) Representative example of changes in neural noise level in the STN and SNr. (B) Changes of MSD in the STN and SNr at different cut-off levels in the same case as shown in A. The cut-off level was varied from 1.2- to 2.0-fold the neural noise level in the IC. The MSD increased at 5 mm from the point where the recording was initiated, and decreased at the tentative target point (10 mm). A cutoff level of 1.2-fold revealed the clearest changes. IC, internal capsule; MSD, multiple-cell spike density; SNr, pars reticulata of the substantia nigra; STN, subthalamic nucleus.

Change in Multiple-Cell Spike Density Along the Trajectory

The MSD clearly increased when the electrode crossed the dorsal boundary of the STN, and decreased when the electrode passed through the ventral boundary of the STN and entered the SNr. The MSD within the STN was large as compared to that in the IC or ZI and that in the SNr at any cut-off level ranging from 1.2- to 2.0-fold (Fig. 5B). The cut-off level of 1.2-fold revealed the largest increase in MSD in the STN (554 ± 201 spikes/s), which was markedly higher than the MSD in the IC or ZI (19 ± 11 spikes/s; $p < 0.0001$, $N = 90$) and SNr (106 ± 77 spikes/s; $p < 0.0001$, $N = 90$) at this cut-off level. The dorsal and ventral boundaries of the STN were clearly identified from the increase and decrease in the MSD, respectively, in all of the 90 sides.

Along the trajectory of the semimicroelectrode, we divided the STN into 4 parts equally, and named them sequentially as part 1 to part 4 in the direction from the most anterodorsal part (part 1) to the most posteroventral part (part 4). The MSD was the lowest in part 4 (404 ± 130 spikes/s) as compared to part 1 (560 ± 185 spikes/s; $p < 0.0001$, $N = 90$), part 2 (601 ± 226 spikes/s; $p < 0.0001$, $N = 90$) and part 3 (543 ± 205 spikes/s; $p < 0.0001$, $N = 90$; Fig. 6). Nevertheless, the MSD in the SNr (see

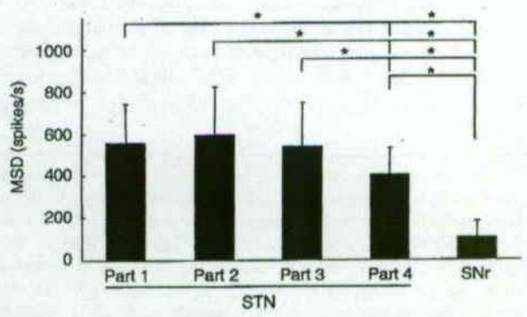

FIGURE 6. Changes in MSD within the STN and SNr. The trajectory passing through the STN was divided equally into 4 parts. The parts were named in such a way that the most anterodorsal part of the STN was part 1, and the most posteroventral part of the STN was part 4. The MSD was lower in part 4 as compared to any of the other parts. The MSD in the SNr was the lowest, as compared to any of the four parts within the STN, $*p < 0.0001$. MSD, Multiple-cell spike density; SNr, pars reticulata of the substantia nigra; STN, subthalamic nucleus.

above) was low even as compared to that of part 4 of the STN ($p < 0.0001$, $N = 90$).

The initial tracking correctly targeted the STN in 40 (88.9%) of the 45 initially operated sides (number of trackings, 1.1 ± 0.4; length of the STN at final tracking, 6.0 ± 1.2 mm) and in 42 (93.3%) of the 45 contralateral sides (number of trackings, 1.1 ± 0.3; length of the STN at final tracking, 5.8 ± 1.1 mm). Two or more trackings were needed in the remaining sides. In total, 82 (91.1%) of the 90 initial trackings correctly targeted the STN (number of trackings, 1.1 ± 0.3).

Discussion

Dorsal Boundary of the Subthalamic Nucleus

The present study demonstrated that the neural noise level and MSD clearly increased when the electrode entered the STN. Hutchison et al. (12) reported that when the microelectrode entered the STN, cells generating large amplitude spikes were encountered. In the typical recording within the STN reported by Starr et al. (10), large amplitude spikes from multiple cells and elevated neural noise levels can be seen. The increases in neural noise level and MSD at the dorsal boundary of the STN are consistent with these findings. It appears that the neural noise level and MSD reflect the discharge rate of multiple cells on average and the cell density.

The present study also revealed that the neural noise level in some cases decreased gradually in the posteroventral part of the STN. In addition, the MSD was lower in this part as compared to the rest of the STN. It has been reported that the cellularity of the STN is homogenous in the monkey (22). Sterio et al. (23) found by microelectrode recording, however, that the cell density, estimated from the encountered single cell activity, was lower in the ventral part of the STN (4.7 ± 1.8 cells/mm) as compared to the dorsal part of the STN (6.8 ± 2.0 cells/mm), and the discharge rate of cells was lower in the ventral part of the STN (43 ± 9.5 Hz) as compared to the dorsal part of the STN (52 ± 12 Hz). The gradual decrease in neural noise and relatively lower MSD in the posteroventral part of the STN are consistent with these findings, again indicating that they efficiently reflect both the discharge rate of multiple cells on average and the cell density.

Ventral Boundary of the Subthalamic Nucleus

The discharge rate of STN cells is approximately half the discharge rate of SNr cells, if analyzed as the single cell activity by microelectrode recordings. Hutchison et al. (12) reported that while STN cells show discharges with an irregular pattern at varying rates ranging from 25 to 45 Hz (37 ± 17 Hz), SNr cells exhibit discharges with a more regular pattern at a much faster rate (71 ± 23 Hz). The illustration in their report indicates that the background multiple cell activities are higher in the SNr than in the STN. Starr et al. (10) also reported that cells in the SNr showed discharges at a faster rate (86 ± 16 Hz) as compared to cells in the STN (34 ± 14 Hz).

In contrast to these previous data obtained by microelectrode recording, the neural noise level and MSD were always higher in the STN than in the SNr in the present study. The background multiple cell activities may vary in microelectrode recording depending on the location of the electrode tip. The discrepancy in spike density (discharge rate) between studies employing microelectrodes and semimicroelectrodes appears to reflect a difference in the capability of detecting information regarding the cell density in addition to the discharge rate of cells on average.

Targeting by Semimicroelectrode Recording

The present results demonstrated that the ventral boundary was not always identifiable from the neural noise level alone, because it begins to decrease in the posteroventral part of the STN. In contrast, the dorsal and ventral boundaries of the STN were always identified by MSD analysis with appropriate tracking, indicating that MSD analysis is more important for determining the boundaries of the STN. Although there was no anatomical verification, these functionally defined boundaries represent the most important information for appropriate placement of the DBS electrode within the STN.

In the present study, the lowest cut-off level of 1.2-fold revealed the largest changes. This is clearly because the MSD at such a cut-off level includes fluctuations of the field potential that becomes larger in amplitude within the STN. Because the increase in amplitude of the field potential may also reflect an increase in multiple cell activities as well as the cell density, the significance of MSD analysis may not differ at any cut-off level for determining the boundaries of the STN.

It has been reported that detection of movement-related cells is important for the identification of the dorsolateral part of the STN, and the DBS electrode should be placed in this region (11,14,24). It is not readily possible to isolate such cells with a semimicroelectrode, which may be the only major drawback of the use of a semimicroelectrode.

If the DBS electrode is placed too lateral, however, the stimulation current may spread to the corticospinal tract. We therefore examined by stimulation whether or not the electrode is too close to the lateral boundary of the STN. The distance of the DBS electrode from the midline, as measured on postoperative MRI (see Materials and Methods), in the present series of patients was the same as the distance reported previously by others (11–12 mm) (8,10).

Conclusion

The present study suggests that MSD analysis by semimicroelectrode recording represents a useful, practical, and apparently reliable means for identifying the boundaries of the STN.

Acknowledgments

This work was supported by Grants-in-Aid for Scientific Research from the Ministry of Education, Culture, Sports, Science, and Technology, Japan (Nos. A12307029 and A15209047), Technology for the promotion of the industry-university collaboration at Nihon University, Japan, and a Program Grant from the Ministry of Health, Labor, and Welfare, Japan.

References

1. Katayama Y, Kasai M, Oshima H et al. Subthalamic nucleus stimulation for Parkinson's disease: benefits observed in levodopa-intolerant patients. *J Neurosurg* 2001;95:213–221.
2. Krack P, Batir A, Van Blercom N et al. Five-year follow-up of bilateral stimulation of the subthalamic nucleus in advanced Parkinson's disease. *N Engl J Med* 2003;349:1925–1934.
3. Limousin P, Krack P, Pollak P et al. Electrical stimulation of the subthalamic nucleus in advanced Parkinson's disease. *N Engl J Med* 1998;339:1105–1111.
4. The Deep-Brain Stimulation for Parkinsonís Disease Study Group. Deep-brain stimulation of the subthalamic nucleus or the pars interna of the globus pallidus in Parkinson's disease. *N Engl J Med* 2001;345:956–963.
5. Abosch A, Hutchison WD, Saint-Cyr JA, Dostrovsky JO, Lozano AM. Movement-related neurons of the subthalamic nucleus in patients with Parkinson's disease. *J Neurosurg* 2002;97:1167–1172.
6. Cuny E, Guehl D, Burbaud P, Gross C, Dousset V, Rougier A. Lack of agreement between direct magnetic resonance imaging and statistical determination of a subthalamic target: the role of electrophysiological guidance. *J Neurosurg* 2002;97:591–597.
7. Guridi J, Rodriguez-Oroz MC, Lozano AM et al. Targeting the basal ganglia for deep brain stimulation in Parkinson's disease. *Neurology* 2000;55 (Suppl. 6):S21–S28.
8. Hamid NA, Mitchell RD, Mocroft P, Westby GW, Milner J, Pall H. Targeting the subthalamic nucleus for deep brain stimulation. Technical approach and fusion of pre- and postoperative MR images to define accuracy of lead placement. *J Neurol Neurosurg Psychiatry* 2005;76:409–414.
9. Priori A, Egidi M, Pesenti A et al. Do intraoperative microrecordings improve subthalamic nucleus targeting in stereotactic neurosurgery for Parkinson's disease? *J Neurosurg Sci* 2003;47:56–60.
10. Starr PA, Christine CW, Theodosopoulos PV et al. Implantation of deep brain stimulators into the subthalamic nucleus: technical approach and magnetic resonance imaging-verified lead locations. *J Neurosurg* 2002;97:370–387.
11. Starr PA, Vitek JL, DeLong M, Bakay RA. Magnetic resonance imaging-based stereotactic localization of the globus pallidus and subthalamic nucleus. *Neurosurgery* 1999;44:303–313.
12. Hutchison WD, Allan RJ, Opitz H et al. Neurophysiological identification of the subthalamic nucleus in surgery for Parkinson's disease. *Ann Neurol* 1998;44:622–628.
13. Zonenshayn M, Rezai AR, Mogilner AY, Beric A, Sterio D, Kelly PJ. Comparison of anatomic and neurophysiological methods for subthalamic nucleus targeting. *Neurosurgery* 2000;47:282–292.
14. Rodriguez-Oroz MC, Rodriguez M, Guridi J et al. The subthalamic nucleus in Parkinson's disease: somatotopic organization and physiological characteristics. *Brain* 2001;124:1777–1790.
15. Lanotte MM, Rizzone M, Bergamasco B, Faccani G, Melcarne A, Lopiano L. Deep brain stimulation of the subthalamic nucleus, anatomical, neurophysiological, and outcome correlations with the effects of stimulation. *J Neurol Neurosurg Psychiatry* 2002;72:53–58.
16. Lopez-Flores G, Miguel-Morales J, Teijciro-Amador J et al. Anatomic and neurophysiological methods for the targeting and lesioning of the subthalamic nucleus: Cuban experience and review. *Neurosurgery* 2003;52:817–830.
17. Yamamoto T, Katayama Y, Fukaya C, Oshima H, Kasai M, Kobayashi K. New method of deep brain stimulation therapy with two electrodes implanted in parallel and side by side. *J Neurosurg* 2001;95:1075–1078.
18. Yokoyama T, Sugiyama K, Nishizawa S et al. Neural activity of the subthalamic nucleus in Parkinson's disease patients. *Acta Neurochir (Wien)* 1998;140:1287–1290.
19. Binder DK, Rau G, Starr PA. Hemorrhagic complications of microelectrode-guided deep brain stimulation. *Stereotact Funct Neurosurg* 2003;80:28–31.
20. Yamamoto T, Katayama Y, Kano T, Kobayashi K, Oshima H, Fukaya C. Deep brain stimulation for the treatment of parkinsonian, essential, and poststroke tremor: a suitable stimulation method and changes in effective stimulation intensity. *J Neurosurg* 2004;101:201–209.
21. Yamamoto T, Katayama Y, Kobayashi K, Oshima H, Fukaya C. Dual-floor burr hole adjusted to burr-hole ring and cap for implantation of stimulation electrodes. *J Neurosurg* 2003;99:783–784.
22. Parent A, Hazrati LN. Functional anatomy of the basal ganglia. II. The place of subthalamic nucleus and external pallidum in basal ganglia circuitry. *Brain Res Brain Res Rev* 1995;20:128–154.
23. Sterio D, Zonenshayn M, Mogilner AY et al. Neurophysiological refinement of subthalamic nucleus targeting. *Neurosurgery* 2002;50:58–67.
24. Romanelli P, Heit G, Hill BC, Kraus A, Hastie T, Bronte-Stewart HM. Microelectrode recording revealing a somatotopic body map in the subthalamic nucleus in humans with Parkinson's disease. *J Neurosurg* 2004;100:611–618.

Reprinted from

Journal of Neurosurgery

Direct inhibition of levodopa-induced beginning-of-dose motor deterioration by subthalamic nucleus stimulation in a patient with Parkinson disease

Case report

HIDEKI OSHIMA, M.D., PH.D., YOICHI KATAYAMA, M.D., PH.D., CHIKASHI FUKAYA, M.D., PH.D., TOSHIKAZU KANO, M.D., KAZUTAKA KOBAYASHI, M.D., PH.D., TAKAMITSU YAMAMOTO, M.D., PH.D., AND YUTAKA SUZUKI, M.D., PH.D.

JANUARY 2008 Volume 108, Number 1:160-163

American Association of Neurological Surgeons

WWW.THEJNS.ORG

J Neurosurg 108:160–163, 2008

Direct inhibition of levodopa-induced beginning-of-dose motor deterioration by subthalamic nucleus stimulation in a patient with Parkinson disease

Case report

Hideki Oshima, M.D., Ph.D.,[1,2] Yoichi Katayama, M.D., Ph.D.,[1,2] Chikashi Fukaya, M.D., Ph.D.,[1,2] Toshikazu Kano, M.D.,[2] Kazutaka Kobayashi, M.D., Ph.D.,[2] Takamitsu Yamamoto, M.D., Ph.D.,[1,2] and Yutaka Suzuki, M.D., Ph.D.[1,3]

[1]Division of Applied System Neuroscience, and Departments of [2]Neurological Surgery and [3]Neurology, Nihon University School of Medicine, Tokyo, Japan

✓Beginning-of-dose motor deterioration (BDMD) is a complication of levodopa medications in Parkinson disease (PD) that is presumably caused by inhibitory effects of levodopa. Only limited experience of BDMD has been described in the literature. The authors report the case of a patient with PD who demonstrated a marked BDMD while being treated with standard levodopa medications. This 55-year-old woman had a 12-year history of PD and a 10-year history of levodopa treatment. Marked exacerbation of symptoms occurred 15 to 20 minutes after every dose of levodopa at 100 mg and lasted approximately 15 minutes. The PD symptoms, particularly tremor and rigidity, were exacerbated more markedly during this period than during the wearing-off deterioration. The BDMD could be controlled very well by subthalamic nucleus (STN) stimulation without any change in the regimen of levodopa medications. These observations suggest that the BDMD was inhibited by STN stimulation through a direct effect.
(DOI: 10.3171/JNS/2008/108/01/0160)

Key Words • **deep brain stimulation** • **inhibitory effect** • **levodopa** • **motor fluctuation** • **Parkinson disease** • **subthalamic nucleus**

On-off fluctuation of motor symptoms, which follows exposure to chronic, repetitive administration of levodopa medications, often complicates levodopa therapy in patients with advanced PD. End-of-dose or "wearing-off" motor deterioration parallels the fall in plasma concentration of levodopa.[3,17] In addition, end-of-dose motor deterioration caused by inhibitory effects of levodopa plunges patients into a worsening of disability from their baseline off-medication motor status.[2,16] In 1992, Merello and Lees[12] first reported that some patients with PD also demonstrate motor deterioration, presumably through similar inhibitory effects of levodopa on the rising phase of the plasma levodopa concentration.[6,11–13,16] This phenomenon was designated as "beginning-of-dose motor deterioration,"[12] abbreviated in the present paper as BDMD.

Stimulation of the STN can ameliorate on-off motor fluctuations,[1,4,8–10,14] by attenuating the wearing-off motor deterioration.[18] This effect of STN stimulation is similar to the effects of a maximal dose of levodopa in each patient.[1,4,8,9,14,18] In contrast, little is yet known regarding the influence of STN stimulation on the motor deterioration caused by inhibitory effects of levodopa. We report on a patient with PD who demonstrated a marked BDMD under standard levodopa medications, which was found to be inhibited directly by STN stimulation withstanding levodopa medications.

Abbreviations used in this paper: BDMD = beginning-of-dose motor deterioration; PD = Parkinson disease; STN = subthalamic nucleus; UPDRS = Unified Parkinson's Disease Rating Scale.

Case Report

History and Presentation. This 55-year-old woman had a 12-year history of PD and a 10-year history of levodopa treatment. Although her PD symptoms had progressively worsened, she was being treated with a restricted dose of levodopa because of levodopa-induced hallucinations: 400/40 mg levodopa/dopa-decarboxylase (100/10 mg four times daily), 750 μg pergolide mesylate (250 μg three times daily), and 10 mg selegiline hydrochloride per day. She eventually developed medically uncontrollable on-off motor fluctuations and came to experience BDMD as well as levodopa-induced dose-onset dyskinesia. For these reasons, she was referred to us for STN stimulation.

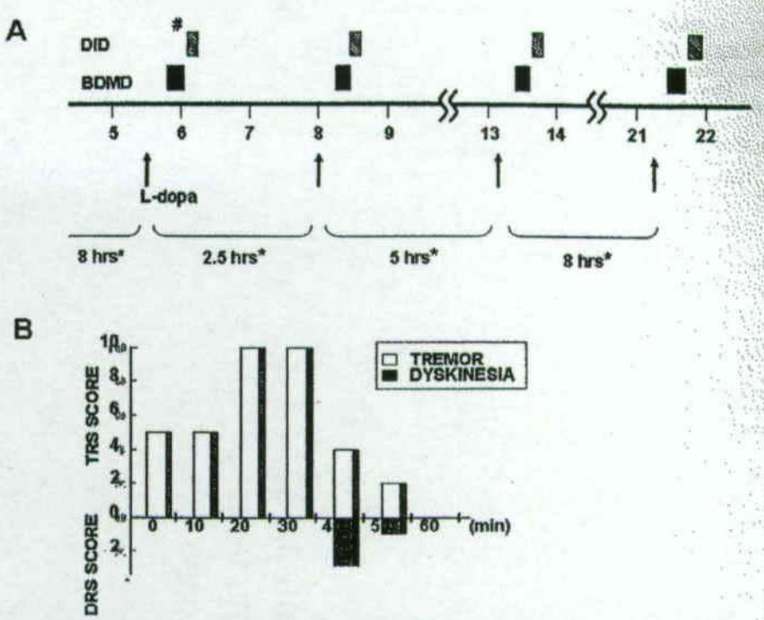

Fig. 1. A: Graph showing the temporal relationship between BDMD and dose-onset dyskinesia (DID) in a patient with PD after administration of levodopa (L-dopa). The *asterisks* indicate intervals from the previous dose of levodopa in hours. B: Temporal relationship between the appearance of tremor in BDMD and dose-onset dyskinesia after an early-morning levodopa dose (indicated by *number sign* in A). DRS = dyskinesia rating scale; TRS = tremor rating scale.

When the patient presented to us the total duration of the off-medication period reached 50% of the day. She complained that the BDMD always appeared after every dose of levodopa.

Presurgical Evaluation. During 2 days of observation, we confirmed that the BDMD occurred at 15 to 20 minutes after every dose of levodopa at 100 mg and lasted for approximately 15 minutes, while the intervals from the previous dose of levodopa varied in the range from 2.5 to 8 hours (Fig. 1). The severity of the BDMD was variable, and the BDMD after the first dose of levodopa in the early morning was apparently most severe (Fig. 1B, Table 1). Exacerbation of the PD symptoms, particularly the tremor and rigidity, which predominated in the lower extremities, was noticeably worse during the BDMD than during the wearing-off period. The motor (Part III) score on the UPDRS was increased during the BDMD by 188% from the score during the best on-medication motor condition (on period) and by 44% from the score during the wearing-off motor deterioration (off period). The BDMD was followed by levodopa-induced dose-onset dyskinesia, which consisted of dystonic posture and pain in the left lower extremity (Fig. 1). The temporal relationship between the BDMD and dyskinesia was uniform, the onset and peak of the BDMD always preceded those of the dyskinesia by 15 to 20 minutes. These clinical findings were consistent with the characteristics of BDMD described in the literature.[12] It was impossible to attribute such short-lived motor deterioration to a continuation of wearing-off or end-of-dose motor deteriorations, since it occurred abruptly and invariably after every dose of levodopa, despite varying intervals between doses.

Surgery and Postsurgical Course. The patient underwent implantation of electrodes (Model 3387, Medtronic, Inc.) and pulse generators for deep brain stimulation of the STN bilaterally. The PD symptoms were greatly improved by bipolar STN stimulation, especially during the off periods, at intensities ranging from 2.0 to 2.5 V (pulse width 180 μsec, frequency 135 Hz) during the follow-up period. Subsequent to the initiation of STN stimulation, the doses of medication were reduced to 200/20 mg levodopa/dopa-decarboxylase, 750 μg pergolide mesylate, and 10 mg selegiline hydrochloride per day. The medications were not completely withdrawn, because the patient reported some motor deterioration in the afternoon (lasting approximately 30 minutes). We confirmed that the BDMD was still induced by every dose of levodopa at 100 mg if the STN stimulation was kept turned off, and was immediately attenuated when the STN stimulation was turned on at intensities of > 1.8 V. Complete inhibition of the BDMD was achieved at intensities of > 2.5 V.

Standard follow-up evaluation at 6 months after surgery revealed that the UPDRS motor score was markedly improved by bilateral STN stimulation at an intensity of 2.0 V during the off period as well as the on period (78 and 75%, respectively; Table 1). The dose-onset dyskinesia disappeared completely. The BDMD was controlled almost com-

TABLE 1

*Preoperative and postoperative UPDRS scores**

UPDRS Measure (max score)	Preop			Postop (% impr‡)		
	Off			6 Mos		
	On	WO	BDMD (% deter†)	On	Off	12 Mos§
ADL (52)	3	17	19 (12)	2 (33)	5 (74)	2
motor (108)	16	32	46 (44)	4 (75)	10 (78)	5
tremor (20)	0	5	10 (100)	0	2 (80)	0
rigidity (20)	5	8	12 (50)	1 (80)	1 (92)	1
akinesia (32)	7	11	13 (18)	0 (100)	2 (85)	1
posture (8)	0	2	2 (0)	0	1 (50)	0
gait (4)	0	1	2 (50)	0	0 (100)	0

* ADL = activity of daily living; deter = deterioration; impr = improvement; Off = off period; On = on period; WO = wearing-off period.

† Percentage deterioration compared with wearing-off.

‡ Percentage improvement compared with before surgery.

§ No off-medication assessment was performed at the 12-month follow-up evaluation because a "no off-medication" condition had been achieved.

pletely, leaving occasional slight and transient tremor in the lower extremities. The results of this evaluation confirmed that the immediate effect of STN stimulation on the BDMD had remained unchanged. The improvement had lasted and a "no off-medication" motor condition had been achieved at 12 months after surgery. We attempted a dopa challenge test (100 mg/10 mg levodopa/dopa-decarboxylase administered orally) at 14 months postoperatively, but BDMD did not occur.

Discussion

Merello and Lees[12] reported BDMD occurring at 10 to 20 minutes after intake of levodopa and lasting for 10 to 20 minutes. Before their report, this phenomenon had been regarded as part of wearing-off or end-of-dose motor deterioration that continued until the next dose of levodopa.[3,16]

Although it has been suggested that BDMD might be common,[12] only limited experience of it has been described in the literature.[6,11–13,16] It appears possible that BDMD can be confused with coexisting levodopa-induced dose-onset dyskinesia.[12] In addition, most cases of BDMD have been detected previously under intentional pharmacological examinations, so it remains unknown how common BDMD might be in patients receiving standard levodopa medications. The present case suggests that a marked BDMD similar to the BDMD observed in intentional pharmacological examinations[12,13] can also occur in patients receiving standard doses of levodopa medications.

Beginning-of-dose motor deterioration has been accounted for on the basis of the inhibitory effects of levodopa, which suppress endogenous dopamine release and synthesis through predominant activation of presynaptic dopamine autoreceptors.[19,20,22] This hypothesis implies that BDMD may be induced by a dose of levodopa that is insufficient to activate postsynaptic dopamine receptors.[12,16] Management of BDMD may therefore be difficult in patients who are already receiving a relatively large dosage of levodopa, and when reducing the levodopa dosage in patients who are distressed by various side effects of the drug.

To the best of our knowledge, the present case demonstrates for the first time that BDMD can be inhibited by STN stimulation and further indicates the benefit of STN stimulation for managing the inhibitory effects of levodopa, if they are in fact responsible for the BDMD. In patients with PD, intraoperative microrecording has revealed that intravenous administration of apomorphine induces increased neuronal activities in both the STN[11] and the internal segment of the globus pallidus[7,13] during BDMD[11,13] and end-of-dose motor deterioration.[7] Such increased neuronal activities are also observed during wearing-off motor deterioration but are quantitatively more pronounced in that setting.[7,11,13] These findings suggest that motor deterioration in patients with PD is closely related to the activities of the basal ganglia, which result in an enhanced inhibitory input to the thalamus. Stimulation of the STN is suggested to suppress such abnormal neuronal activities underlying the PD symptoms[23] and to release the thalamus from excessive inhibition by the basal ganglia.[5,21] It is possible that BDMD and wearing-off motor deterioration are inhibited by STN stimulation through the same mechanism. The precise process whereby STN stimulation can improve on-off motor fluctuation remains to be elucidated. Both presynaptic and postsynaptic mechanisms have been postulated.[15,18] In a study on the interaction between deep brain stimulation and levodopa by Nutt et al.,[18] the improvement effect of acute STN stimulation (when patients were awake during the day) on wearing-off motor fluctuation was inferred to be due to a reduction of off-drug disability, and not alterations in the levodopa pharmacodynamics. This may suggest that the action of STN stimulation may be independent of striatal dopamine transmission; namely, a postsynaptic mechanism is primary. In contrast, Nimura et al.[15] demonstrated that chronic STN stimulation can induce stabilization of the striatal synaptic dopamine concentrations based on an [^{18}F]fluorodopa positron emission tomography study, and levodopa-related wearing-off motor fluctuation may thus be attenuated. The results of the positron emission tomography study indicate that the stabilization induced by STN stimulation involves a presynaptic mechanism. This is assumed to incorporate the following two main processes: 1) activated output from the motor and premotor cortex, which is induced by relaxant output from the STN via the pallidothalamocortical pathway, tending to attenuate dopamine release in the striatum, and 2) restoration of autoregulation in striatal presynaptic dopamine release through a feedback input from the STN to striatal somatodendritic autoreceptors. We inferred that a reduction of levodopa dosage may also contribute stability of striatal dopamine transmission. These combined mechanisms could facilitate further improvement in dopa-induced motor fluctuations with chronic STN stimulation.

Conclusions

The present case confirms that STN stimulation can provide benefits in improving off-medication motor status through levodopa-like effects, through improving the on-medication motor status in patients who are intolerant to larger doses of levodopa, and through reducing the levodopa dose in patients who are distressed by various side effects of levodopa.[8] In addition, our observations suggest that STN stimulation has direct effects on some of the levodopa-induced motor symptoms, such as BDMD. The combination of chronic STN stimulation and reduction in dosage of levodopa may contribute further by improving levodopa-induced motor fluctuations through the stabilization of striatal dopamine transmission.

References

1. Burchiel KJ, Anderson VC, Favre J, Hammerstad JP: Comparison of pallidal and subthalamic nucleus deep brain stimulation for advanced Parkinson's disease: results of a randomized, blinded pilot study. **Neurosurgery 45:**1375–1382, 1999
2. Contin M, Riva R, Martinelli P, Procaccianti G, Cortelli P, Avoni P, et al: Response to a standard oral levodopa test in Parkinsonian patients with and without motor fluctuations. **Clin Neuropharmacol 13:**19–28, 1990
3. Davis TL, Brughitta G, Baronti F, Mouradian MM: Acute effects of pulsatile levodopa administration on central dopamine pharmacodynamics. **Neurology 41:**630–633, 1991
4. Deep-Brain Stimulation for Parkinson's Disease Study Group: Deep-brain stimulation of the subthalamic nucleus or the pars interna of the globus pallidus in Parkinson's disease. **N Engl J Med 345:**956–963, 2001
5. Hashimoto T, Elder CM, Okun MS, Patrick SK, Vitek JL: Stimulation of the subthalamic nucleus changes the firing pattern of pallidal neuron. **J Neurosci 23:**1916–1923, 2003
6. Hughes AJ, Lees AJ, Stern GM: Apomorphine test to predict dopaminergic responsiveness in parkinsonian syndromes. **Lancet 336:**32–34, 1990
7. Hutchinson WD, Levy R, Dostrovsky JO, Lozano AM, Lang AE: Effects of apomorphine on globus pallidus neurons in parkinsonian patients. **Ann Neurol 42:**767–775, 1997
8. Katayama Y, Kasai M, Oshima H, Fukaya C, Yamamoto T, Ogawa K, et al: Subthalamic nucleus stimulation for Parkinson disease: benefits observed in levodopa-intolerant patients. **J Neurosurg 95:**213–221, 2001
9. Krack P, Batir A, Van Blercom N, Chabardes S, Fraix V, Ardouin C, et al: Five-year follow-up of bilateral stimulation of the subthalamic nucleus in advanced Parkinson's disease. **N Engl J Med 349:**1925–1934, 2003
10. Kumar R, Lozano AM, Kim YJ, Hutchison WD, Sime E, Halket E, et al: Double-blind evaluation of subthalamic nucleus deep brain stimulation in advanced Parkinson's disease. **Neurology 51:**850–855, 1998
11. Levy R, Dostrovsky JO, Lang AE, Sime E, Hutchison WD, Lozano AM: Effects of apomorphine on subthalamic nucleus and globus pallidus internus neurons in patients with Parkinson's disease. **J Neurophysiol 86:**249–260, 2001
12. Merello M, Lees AJ: Beginning-of-dose motor deterioration following the acute administration of levodopa and apomorphine in Parkinson's disease. **J Neurol Neurosurg Psychiatry 55:**1024–1026, 1992
13. Merello M, Lees AJ, Balej J, Cammarota A, Leiguarda R: GPi firing rate modification during beginning-of-dose motor deterioration following acute administration of apomorphine. **Mov Disord 14:**481–483, 1999
14. Moro E, Scerrati M, Romito LM, Roselli R, Tonali P, Albanese A: Chronic subthalamic nucleus stimulation reduces medication requirements in Parkinson's disease. **Neurology 53:**85–90, 1999
15. Nimura T, Yamaguchi K, Ando T, Shibuya S, Oikawa T, Nakagawa A, et al: Attenuation of fluctuating striatal synaptic dopamine levels in patients with Parkinson disease in response to subthalamic nucleus stimulation: a positron emission tomography study. **J Neurosurg 103:**968–973, 2005
16. Nutt JG, Gancher ST, Woodward WR: Does an inhibitory action of levodopa contribute to motor fluctuations? **Neurology 38:**1553–1557, 1988
17. Nutt JG, Holford NHG: The response to levodopa in Parkinson's disease: imposing pharmacological law and order. **Ann Neurol 39:**561–573, 1996
18. Nutt JG, Rufener SL, Carter JH, Anderson VC, Phawa R, Hammerstad JP, et al: Interactions between deep brain stimulation and levodopa in Parkinson's disease. **Neurology 57:**1835–1842, 2001
19. Paalzow GH, Paalzow LK: L-DOPA: how it may exacerbate parkinsonian symptoms. **Trends Pharmacol Sci 9:**15–19, 1986
20. Skirboll LR, Grace AA, Bunney BS: Dopamine auto- and postsynaptic receptors: electrophysiological evidence for differential sensitivity to dopamine agonists. **Science 206:**80–82, 1979
21. Welter ML, Houeto JL, Bonnet AM, Bejjani PB, Mesnage V, Dormont D, et al: Effects of high-frequency stimulation on subthalamic neuronal activity in parkinsonian patients. **Arch Neurol 61:**89–96, 2004
22. Westfall TC, Besson MJ, Giorgulieff MF, Glowinski J: The role of presynaptic receptors in the release and synthesis of ^{3}H-dopamine by slices of rat striatum. **Naunyn Schmiedebergs Arch Pharmacol 292:**279–289, 1976
23. Wichmann T, DeLong MR: Functional and pathophysiological models of the basal ganglia. **Curr Opin Neurobiol 6:**751–758, 1996

Manuscript submitted June 2, 2005.
Accepted May 17, 2007.
This work was supported by grants from the Ministry of Education, Culture, Sports, Science, and Technology (Grant Nos. 12307029 and 15209047) and the Ministry of Education, Culture, Sports, Science, and Technology for the promotion of industry–university collaboration at Nihon University.

Address correspondence to: Hideki Oshima, M.D., Ph.D., Department of Neurological Surgery, Nihon University School of Medicine, Tokyo 173-8610, Japan. email: hoshima@med.nihon-u.ac.jp.

■連載—脳神経外科医療の translational research (6)

脳・神経刺激療法の translational research

深谷　親　　片山　容一

NEUROLOGICAL SURGERY
脳神経外科
(文献略称：No Shinkei Geka)

第35巻 第4号 別刷
2007年4月10日 発行

医学書院

Neuromodulation

Technology at the Neural Interface

VOLUME XI • NUMBER 2 • APRIL 2008

Samuel J. Hassenbusch III, MD, PhD
1954–2008
In Memoriam

Journal of the International Neuromodulation Society

Official Journal of the International Functional Electrical Stimulation Society

Volume 11 • Number 2 • 2008
http://www.blackwell-synergy.com/loi/ner

ORIGINAL ARTICLE

Effect of Subthalamic Nucleus Stimulation on Severe Striatal Hand Deformity in Parkinson's Disease: A Case Report

Takashi Morishita, MD[1,2] • Yoichi Katayama, MD, PhD[1,2] • Kazutaka Kobayashi, MD, PhD[1,2] • Hideki Oshima, MD, PhD[1] • Chikashi Fukaya, MD, PhD[1,2] • Takamitsu Yamamoto, MD, PhD[1,2]

[1]*Division of Neurosurgery, Department of Neurological Surgery, and* [2]*Division of Applied System Neuroscience, Department of Advanced Medical Science, Nihon University School of Medicine, Tokyo, Japan*

ABSTRACT

Striatal hand is a deformity encountered in Parkinson's disease and other parkinsonisms. It is characterized by extension that occurs at all the interphalangeal joints, flexion at the metacarpophalangeal joints, and ulnar deviation. It can be differentiated from levodopa-induced dystonia and primary dystonia, since the deformity exists continuously even during sleep. We experienced a case of Parkinson's disease with severe striatal hand deformity which was successfully treated by deep brain stimulation of the subthalamic nucleus (STN-DBS). Although the precise mechanism remains unclear, rigidity is assumed to contribute to the limb deformities. Based on our experience, it seems possible therefore that the effect of STN-DBS on the hand deformity was a secondary effect on muscular rigidity. STN-DBS is assumed to represent a useful treatment option for striatal hand deformity.

KEY WORDS: *Deep brain stimulation, dystonia, Parkinson's disease, striatal deformity, subthalamic nucleus.*

Introduction

Charcot (1877) first reported the deformities of the hands and feet that are unique to Parkinson's disease (PD) (1). The hand deformities are typically characterized by extension that occurs at all the interphalangeal joints, flexion at the metacarpophalangeal joints, and ulnar deviation. The feet are described as showing claw-like deformities that accompany extension of the first and flexion of the second phalanges. They resemble rheumatoid arthritis, but do not display osteogenic changes and are negative for rheumatoid factor. Similar deformities can also be seen in other parkinsonisms which involve neostriatal pathophysiological abnormalities such as multiple system atrophy, progressive supranuclear palsy, and corticobasal degeneration, and they are thus called striatal hand or foot. Ashour et al. suggested that the terms striatal hand and foot be used to describe the features of these distal limb deformities in parkinsonism (2). Striatal limb deformity can be the first sign of PD, and is therefore differentiated from dopa-induced dystonia. Primary dystonia is often induced by action. On the other hand, striatal deformities exist continuously even during sleep. However, it remains still controversial as to whether the deformity constitutes primary dystonia or not (2,3).

Submitted: April 8 2007, 2006; accepted: July 31, 2007. Address correspondence and reprint requests to: Takamitsu Yamamoto, MD, PhD, Department of Neurological Surgery, Nihon University School of Medicine, 30-1 Oyaguchi Kamimachi, Itabashi-ku, Tokyo 173-8610, JAPAN. Email: nusmyama@med.nihon-u.ac.jp

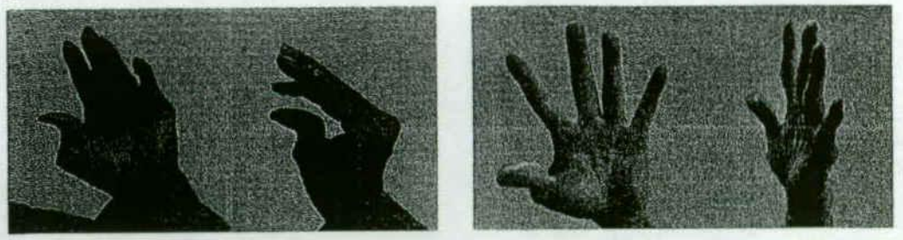

FIGURE 1. Left hand posture before deep brain stimulation of the subthalamic nucleus (STN-DBS) (A) and three years after STN-DBS (B). The patient could not extend the interdigital spaces before STN-DBS. However, after STN-DBS, he could open his palm easily and extend the interdigital spaces.

These deformities are clinically important in terms of the patient's activities of daily living and quality of life. There have been reports concerning various treatment options, such as botulinum toxin (4), orthopedic surgical interventions (5), and stereotactic thalamotomy (6). Deep brain stimulation (DBS) is now regarded as one of the effective treatment options for PD, and an effect on bradykinesia, rigidity, tremor, and dyskinesia has been demonstrated. To the best of our knowledge, there have been few reports focusing on the effect of DBS of the subthalamic nucleus (STN) on striatal hand deformity. Among our over 300 cases of STN-DBS, we have experienced several cases of PD with striatal limb deformities. We describe here a case of PD with one of the severest hand deformities which was treated by chronic STN-DBS.

Case Report

The patient was a 79-year-old man who had remained in his usual state of health until 1997, when he noticed deformity of his left hand first, and tremor occurred later on. He was diagnosed as having PD, and antiparkinsonian drugs were initiated in 1998. His symptoms progressed gradually to include motor fluctuations and wearing-off periods. He was intolerant to levodopa because of gastrointestinal side-effects, so he was able to receive a small dose of antiparkinsonian drugs. Finally, he was referred to our hospital and admitted for an operation in March 2004.

On admission, the patient's Hoehn and Yahr stage and the Unified Parkinson's Disease Rating Scale (UPDRS) were evaluated with optimal medications (7). His Hoehn and Yahr stage during the on period was III and that during the off period was IV. His total UPDRS scores during the on and off periods were 35 and 48, respectively. Based on these results, he was adjudged to be a good candidate for STN-DBS.

On examination, he displayed severe resting tremor and rigidity that were dominant on the left side. He also had deformity of his left hand (Fig. 1A) and was unable to hold anything with his left hand. The interphalangeal joints were extended and the metacarpophalangeal joints were flexed. The range of motion was restricted in the metacarpophalangeal joints of the left hand. Ulnar deviations were remarkable in the fifth finger of the left hand, and the deformity of the thumb exhibited fixed contracture. A hand X-ray showed none of the osteogenic changes that should be seen in rheumatoid arthritis, but dislocation of the distal interphalangeal joint of the thumb was observed (Fig. 2A). The deformity existed at rest even during sleep. Nerve conduction studies revealed that the peripheral nerves were intact. The deformity could be distinguished from dopa-induced dystonia because of the observed history in which the deformity represented the first sign of PD, was fixed and did not respond to levodopa. Based on these findings, the hand deformity was diagnosed as striatal hand. The hand deformity was given a score of 4 on the scale of 0–4 according to the striatal hand rating scale (8).

Following bilateral STN-DBS, the tremor, rigidity, and motor fluctuations were alleviated and the wearing-off periods disappeared. The Hoehn and Yahr stage improved to I even during the off periods, and the total UPDRS scores were also dramatically improved: 16 during the on period and 18 during the off period, at one year after the surgery. The rigidity underwent improvement as shown in Table 1. In addition, the levodopa equivalent dose was reduced from 330 mg to 210 mg. The deformity could be distinguished from dopa-induced dystonia because of the observed history. The deformity represented the first sign of PD. In addition, the deformity was fixed and did not respond to levodopa. The joints of the left hand, especially the metacarpophalangeal joints, became straightened; and the range of motion of the left hand was increased. The striatal hand rating scale improved to 1. The patient is now able to pick up small objects with his left hand.

Discussion

Ashour et al. reported that 12.8% of patients with PD encountered striatal deformities (8), and the deformities

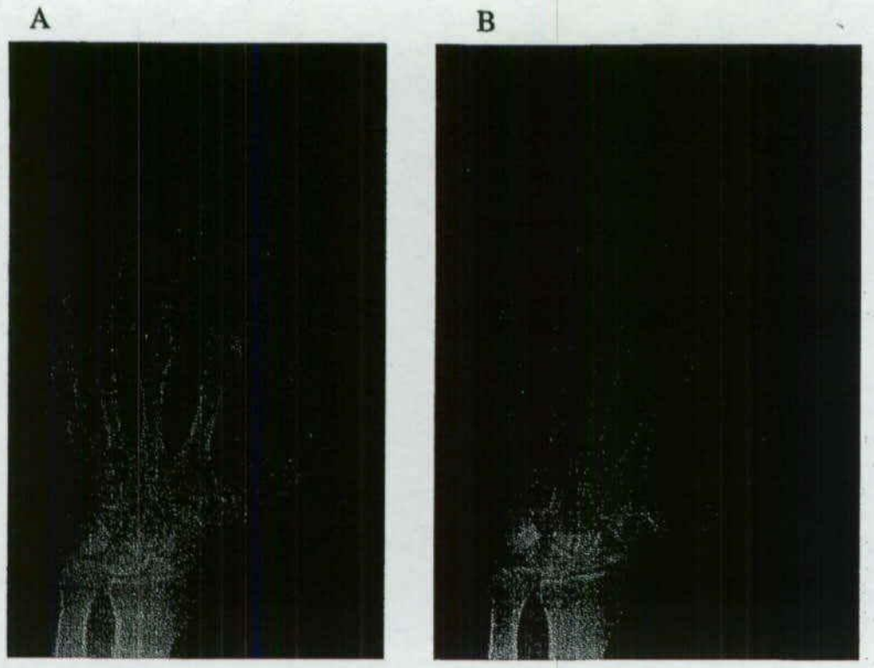

FIGURE 2. Left hand X-ray examinations before deep brain stimulation of the subthalamic nucleus (STN-DBS) (A) and three years after STN-DBS (B). Although the dislocated distal interphalangeal joint of the thumb did not show improvement due to fixed contracture, the interdigital spaces were clearly expanded after STN-DBS.

TABLE 1. Clinical Evaluations Before and After Deep Brain Stimulation of the Subthalamic Nucleus (STN-DBS)

	Before		One year after	
	On period	Off period	On period	Off period
Hoehn and Yahr stage	III	IV	II	II
Total UPDRS	35	48	16	18
UPDRS Part III	22	31	12	12
Item 22 (Rigidity)	10	10	0	0
Striatal hand rating scale	4		1	
Levodopa equivalent dose	330 mg		210 mg	

The Hoehn and Yahr stage, the Unified Parkinson's Disease Rating Scale (UPDRS), striatal hand rating scale, and levodopa equivalent dose were evaluated before and at one year after STN-DBS. A remarkable improvement was seen in the motor scores.

can be presented at the early stages of PD (1,8). Rigidity caused by lesions in the neostriatum has been considered to contribute to the etiology of the deformities as mentioned by Gowers (9), and another report has supported the existence of a correlation between rigidity and the deformities (10). Although the mechanism of the effect of STN-DBS on such deformity is unclear, improvement of the rigidity may contribute to the improvement of the deformity since we experienced dramatic improvement of rigidity as well as improvement of the hand deformity.

It is well known that certain dystonic postures besides striatal limb deformities and dopa-induced dystonic dyskinesia occur in PD (3). Striatal deformities are atypical for dystonia and classified as one of the atypical dystonias in PD (3). Striatal deformities exist continuously even during sleep. In contrast, primary dystonia does not present during sleep but is usually induced or exacerbated by a particular action or posture (2). In addition, striatal deformity usually accompanies other parkinsonian signs and symptoms. A long history of dystonia can also lead to fixed contracture, and, in this respect, it is difficult to distinguish striatal deformities from dystonia. As Chou described in a case of cervical dystonia successfully treated by STN-DBS (11), it is possible that STN-DBS is effective on dystonic pathophysiology. Therefore, it is possible that STN-DBS can be also effective for a dystonic etiology in our case.

Poewe et al. hypothesized that striatal somatotopic organization relates to rostrocaudal gradient of decreased dopamine and increased γ-aminobutyric acid in PD patient with dopa-induced dyskinesia (12) based on clinical experience and animal studies (13,14). Similarly, the relationship between rostrocaudal gradient of dopamine and somatotopy in the striatum might correlate with the fact that the deformities tend to occur in the distal part of the limb. A recent functional magnetic resonance imaging study also described the somatotopy in the human striatum (15). In addition, a positron emission tomography study showed increase in regional cerebral blood flow in the prefrontal cortex, putamen, and thalamus in PD patients after STN-DBS (16). Such effect on blood flow may also contribute to the improvement of the deformities.

Some other mechanisms such as an effect by ergot dopamine agonist and female hormone have been proposed. In our case, the hand deformity existed continuously even during sleep. In addition, our patient did not take ergot dopamine agonist and was a male.

The timing of initiating surgery for PD patients with limb deformities seems to be important. Hu et al. reported a PD patient with right upper limb contracture that was refractory to unilateral ventromedial pallidotomy (17). They described the patient as showing "moderate improvement in dyskinesias and 'off' period symptoms, but no change in the hand-arm contractures." They inferred that the timing of the pallidotomy was too late to improve the deformities. In this context, it may well be true that we initiated the STN-DBS in our case before the joint had reached contracture.

Improvement of motor function correlates with the quality of life of patients with PD. At the same time, improvement in the deformities is thought to contribute to improving the quality of life of such patients. STN-DBS is usually indicated for patients with advanced PD such as cases with severe side-effects of levodopa therapy. On the other hand, the deformities can be encountered even at the early stage of PD as we experienced, and they make the patient's quality of life worse. STN-DBS may thus be indicated in PD patients with limb deformities even at the early stage of their disease if it is resistant to any medications. Nevertheless, further research is needed to evaluate the exact effects and the enrollment of DBS for such deformities.

References

1. Charcot JM. *Lectures on the Diseases of the Nervous System, Lecture V.* London: New Sydenham Society, 1877.

2. Ashour R, Tintner R, Jankovic J. Striatal deformities of the hand and foot in Parkinson's disease. *Lancet Neurol* 2005;4:423–431.

3. Tolosa E, Compta Y. Dystonia in Parkinson's disease. *J Neurol* 2006;253:7003–7006.

4. Cordivari C, Misra VP, Cattania S, Lees AJ. Treatment of dystonic clenched fist with botulinum toxin. *Mov Disord* 2001;16:907–913.

5. Heinzelmann P, Dow R. Clawhand deformity presumed secondary to Parkinson's disease. *J Hand Surg [Am]* 1985;10:19–21.

6. Gortvai P. Deformities of the hands and feet in parkinsonism and their reversibility by operation. *J Neurol Neurosurg Psychiatry* 1963;26:33–36.

7. Katayama Y, Kasai M, Oshima H et al. Subthalamic nucleus stimulation for Parkinson disease: benefits observed in levodopa-intolerant patients. *J Neurosurg* 2001;95:213–221.

8. Ashour R, Jankovic J. Joint and skeletal deformities in Parkinson's disease, multiple system atrophy, and progressive supranuclear palsy. *Mov Disord* 2006;21:1856–1863.

9. Gowers WR. *A Manual of Diseases of the Nervous System.* Philadelphia: P Blakiston, Son & Co, 1888.

10. Reynolds F, Petropoulous G. Hand deformities in parkinsonism. *J Chronic Dis* 1965;18:593–595.

11. Chou KL, Hurtig HI, Jaggi JL, Baltuch GH. Bilateral subthalamic nucleus deep brain stimulation in a patient with cervical dystonia and essential tremor. *Mov Disord* 2005;20:377–380.

12. Poewe WH, Lees AJ. The pharmacology of foot dystonia in Parkinsonism. *Clin Neuropharmacol* 1987;10:47–56.

13. Künzle H. Bilateral profections from precentral motor cortex to the putamen and other parts of the basal ganglia. An autoradiographic study in *Macaca fascicularis. Brain Res* 1975;88:195–209.

14. Delong MR, Georgopoulos AP, Crucher MD, Mitchell JS, Richardson RT, Alexander GE. Functional organization of the basal ganglia: contributions of single cell recording studies. *Ciba Found Symp* 1984;107:64–82.

15. Gerardin E, Lehericy S, Pochon JB et al. Foot, hand, face and eye representation in the human striatum. *Cereb Cortex* 2003;13:162–169.

16. Thobois S, Dominey P, Frax V et al. Effects of subthalamic nucleus stimulation on actual and imagined movement in Parkinson's disease: a PET study. *J Neurol* 2002;249:1689–1698.

17. Hu MTM, Bland J, Clough C, Ellis CM, Chaudhuri KR. Limb contractures in levodopa-responsive parkinsonism: a clinical and investigational study of seven new cases. *J Neurol* 1999; 246:671–676.

Neuromodulation

Technology at the Neural Interface

VOLUME XI • NUMBER 3 • JULY 2008

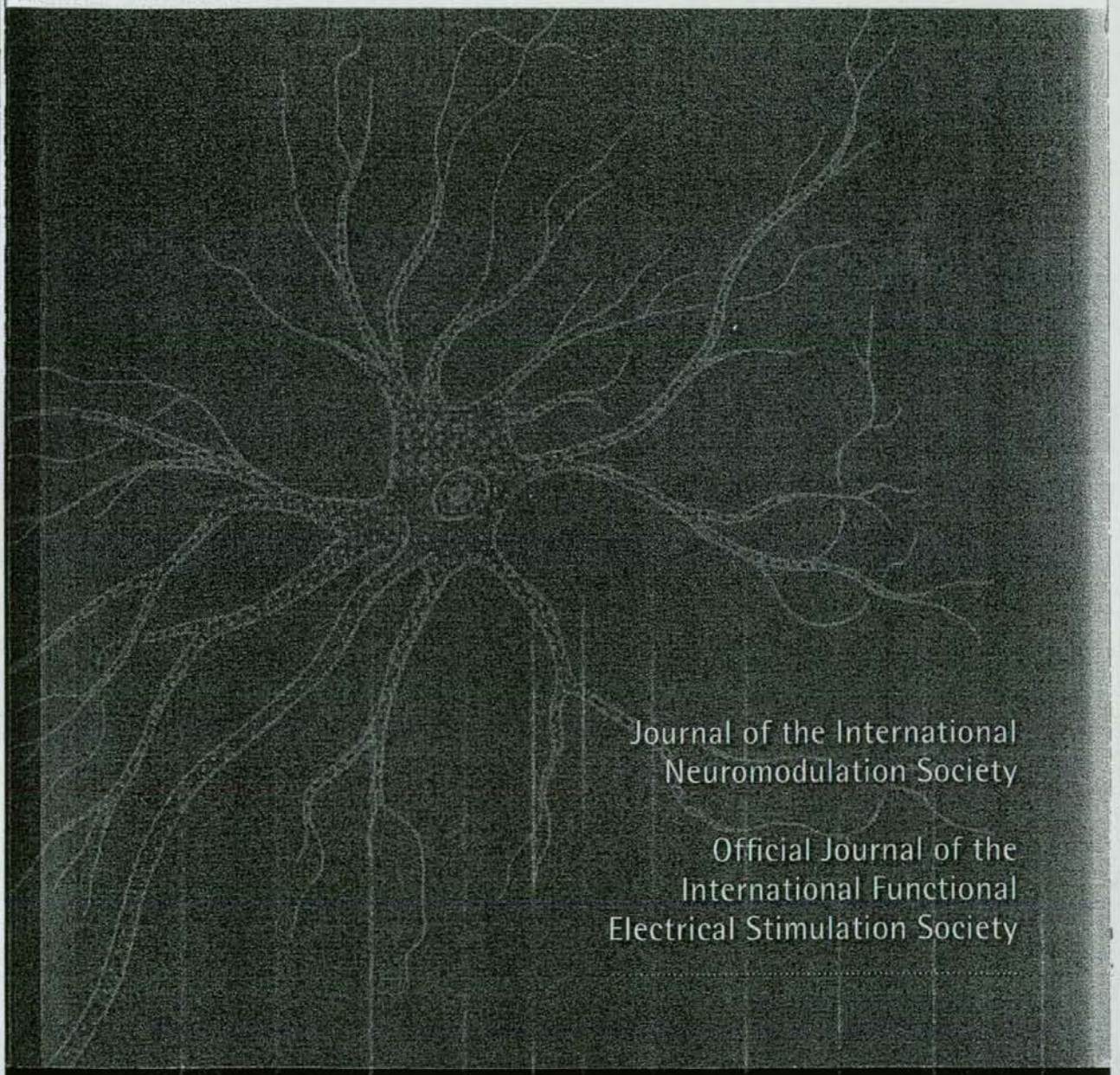

Journal of the International Neuromodulation Society

Official Journal of the International Functional Electrical Stimulation Society